Civil, Architectural and Environmental
Engineering Faculty Research & Creative Works

Civil, Architectural and Environmental
Engineering

01 Nov 2009

Coaxial Cable Sensors and Sensing Instrument for Crack Detection in Bridge Structures -- Phase I: Field Qualification/ Validation Planning

Genda Chen
Missouri University of Science and Technology, gchen@mst.edu

Fujian Tang

Zhi Zhou

Follow this and additional works at: https://scholarsmine.mst.edu/civarc_enveng_facwork

Part of the Structural Engineering Commons

Recommended Citation

COAXIAL CABLE SENSORS AND SENSING INSTRUMENT FOR CRACK DETECTION IN BRIDGE STRUCTURES – PHASE I: FIELD QUALIFICATION/VALIDATION PLANNING

Final Report

Prepared for

THE NEW YORK STATE ENERGY RESEARCH AND DEVELOPMENT AUTHORITY

Albany, NY

Joseph D. Tario

Senior Project Manager

and

THE NEW YORK STATE DEPARTMENT OF TRANSPORTATION

Albany, NY

Norbert Luft

Project Manager

In collaboration with

CENTER FOR TRANSPORTATION INFRASTRUCTURE AND SAFETY, MISSOURI UNIVERSITY OF SCIENCE AND TECHNOLOGY (MISSOURI S&T)

Prepared by

CENTER FOR INFRASTRUCTURE ENGINEERING STUDIES, MISSOURI S&T

Rolla, MO

Genda Chen

Principal Investigator

Fujian Tang and Zhi Zhou

Project Team Members

CONTRACT NOS. 9820 / C-06-34

November 6, 2009

i

NOTICE

DISCLAIMER

TECHNICAL REPORT DOCUMENTATION PAGE

1. Report No. C-06-34	2. Government Accession No.	3. Recipient's Catalog No.
4. Title and Subtitles Coaxial Cable Sensors and Sensing Instrument for Crack Detection in Bridge Structures – Phase I: Field Qualification/Validation Planning	5. Report Date November 6, 2009	
	6. Performing Organization Code Missouri University of Science and Technology	
7. Author/s Genda Chen, Fujian Tang, and Zhi Zhou	8. Performing Organization Report No.	
9. Performing Organization Name and Address Center for Infrastructure Engineering Studies Missouri University of Science and Technology 223 Engineering Research Laboratory Rolla, MO 65409-0710	10. Work Unit No. (TRAIS)	
	11. Contract or Grant No. Contract No. 9820	
12. Sponsoring Organization Name and Address NYS Energy Research and Development Authority 17 Columbia Circle, Albany, NY 12203-6399 NYS Department of Transportation 50 Wolf Road, Albany, NY 12232	13. Type of report and period covered Final Report (June 1, 2008 - October 31, 2009)	
	14. Sponsoring Agency Code	
15. Supplementary Notes This work is completed in collaboration with the Center for Transportation Infrastructure and Safety at Missouri University of Science and Technology, 223 Engineering Research Laboratory, Rolla, MO 65409-0710		

16. Abstract
The objectives of this study are to pre-test analyze a decommissioned RC bridge that is selected in consultation with New York State Department of Transportation (NYSDOT), and design and plan the field tests of the bridge for the performance qualification and validation of distributed crack sensors and a fast Electrical Time Domain Reflectometry (ETDR) instrument to their full potential. The scope of work includes: (a) Selection of a decommissioned bridge, (b) Pre-test analysis of the select bridge structure to evaluate its progressive damage and determine the locations for sensor deployment, (c) Design and planning of field tests of the select bridge, (d) Field instrumentation with coaxial cable and fiber optical sensors for performance comparison, and (d) Summary of the findings of this study. Once fully validated and demonstrated in field conditions, distributed crack sensors and sensing instruments are expected to play a significant role in routine inspections and bridge ratings and in the rapid assessment of structural conditions for post-event evaluations and responses, improving the safety and security of transportation infrastructure at the height of a crisis. These roles are due primarily to their unique ability of permanently recording the widest crack a RC member experienced during a recent event. Such an attribute ensures the availability of damage data even if a fast ETDR system experiences malfunction during the event, greatly improving the reliability of bridge inspections.

17. Key Words Power substation, finite element model, modal analysis, response spectrum analysis, time history analysis, shake table test.	18. Distribution Statement No restrictions.	
19. Security Classification (of this report) Unclassified	20. Security Classification (of this page) Unclassified	21. No. of Pages 36

ABSTRACT

The objectives of this study are to pre-test analyze a decommissioned RC bridge that is selected in consultation with New York State Department of Transportation (NYSDOT), and design and plan the field tests of the bridge for the performance qualification and validation of distributed crack sensors and a fast Electrical Time Domain Reflectometry (ETDR) instrument to their full potential. The scope of work includes: (a) Selection of a decommissioned bridge, (b) Pre-test analysis of the select bridge structure to evaluate its progressive damage and determine the locations for sensor deployment, (c) Design and planning of field tests of the select bridge, (d) Field instrumentation with coaxial cable and fiber optical sensors for performance comparison, and (d) Summary of the findings of this study. Once fully validated and demonstrated in field conditions, distributed crack sensors and sensing instruments are expected to play a significant role in routine inspections and bridge ratings and in the rapid assessment of structural conditions for post-event evaluations and responses, improving the safety and security of transportation infrastructure at the height of a crisis. These roles are due primarily to their unique ability of permanently recording the widest crack a RC member experienced during a recent event. Such an attribute ensures the availability of damage data even if a fast ETDR system experiences malfunction during the event, greatly improving the reliability of bridge inspections.

TABLE OF CONTENTS

LIST OF FIGURES

LIST OF TABLES

NOTATIONS

C	Strain coefficient
n	Refractive index
v_A	Acoustic wave velocity
$v_B(\varepsilon)$	Brillouin frequency shift at strain ε
ε	Strain to be measured by an optical fiber
λ	Wavelength of incident light

1   INTRODUCTION

This report summarizes the findings and results of a Phase I study (PON No.1028) that was focused on the design of field tests on a decommissioned highway bridge in Jamestown, NY. A future Phase II study will execute the field test plan to qualify and validate the performance of a cable sensor and sensing instrument.

The objectives of this Phase I study are to pre-test analyze a decommissioned RC bridge that is selected in consultation with New York State Department of Transportation (NYSDOT), and design and plan the field tests of the bridge for the performance qualification and validation of distributed crack sensors and a fast electrical time domain reflectometry (ETDR) instrument to their full potential. The scope of work includes:
- Selection of a decommissioned bridge,
- Pre-test analysis of the select bridge structure to evaluate its progressive damage and determine the locations for sensor deployment,
- Design and planning of field tests of the select bridge,
- Field instrumentation with coaxial cable and fiber optical sensors for performance comparison, and
- Summary of the findings of this study.

2   PROBLEM STATEMENT

The American Society of Civil Engineers (ASCE) in 2005 gave the nation's infrastructure an average grade of "D", indicating severely deteriorated infrastructure conditions due to aging and environmental effects. Transportation infrastructure alone required an annual spending of $94 billion over the following five years to alleviate potential problems associated with the nation's deteriorated infrastructure. As such, the inspection and maintenance of transportation infrastructures are and will continue to be the main sources of expenditure in most, if not all, of the state Departments of Transportation (DOTs). In the past four years, the infrastructure condition remained the same if not worse.

In the state of New York, over 90% of the road construction program is for infrastructure maintenance and repair. Poor roadway and structural conditions has led to more gasoline consumption associated with slow traffic flows, and could result in disruption of business and economic growth, discomfort of the citizens, and environmental pollution. Cracking in bridge decks due to vehicle-induced vibration also becomes an increasing concern. In addition, the safety and security of bridges due to man-made and natural hazards is a real concern to New York. For example, Au Sable Forks, NY, experienced an M5.1 earthquake on a Richter scale on April 20, 2002. The collapse of the former World Trade Center on September 11, 2001, is another example.

The current practice to assess the structural condition of bridges is visual inspection every two years. This time-based strategy is uneconomical when a bridge is in good condition, and could miss the occurrence of structural damages in between two inspections. Damage in transportation

structures is sometimes hidden beneath the painting of steel structures or behind the column jacketing (steel, concrete, or fiber reinforced polymer), and therefore cannot be detected with visual inspection. If minor damage is not identified in a timely fashion, the consequences could be catastrophic, or the damage could grow to the extent that they require substantially more resources to fix it. For example, fatigue and fracture of one critical steel member could render a non-redundant steel bridge totally unusable. Cracks in reinforced concrete (RC) can lead to larger deflections and provide an avenue for water seepage to corrode reinforcing bars, resulting in a weaker RC structure.

3   POTENTIAL SOLUTION WITH SENSING TECHNOLOGY

The proposed solution for an early and timely warning and response of potential problems in deteriorated bridges is to develop and implement a condition-based inspection strategy so that proper measures can be taken in time to remediate the problems. Not only can such a strategy reduce repair costs due to timely remediation, but it also provides a basis for rapid decision making immediately after a catastrophic event in order to effectively manage post-event response and evaluation at the height of a crisis. In this case, the impact of such a strategy is not only an economic issue but a matter of safety. Following is a presentation of a potential solution in two phases: long-term and short-term. Both coaxial cable sensors and optical fiber sensors will be discussed with the former as a primary sensing technology to be validated in this study.

The long-term solution that will be demonstrated in a future study is a continuous monitoring of bridge conditions with distributed crack sensors, ETDR instruments, and other sensors. It involves the use of a structural health monitoring (SHM) system that generally consists of sensors, data acquisition, a microprocessor with embedded signal processing and damage detection (prognosis/diagnosis) algorithms, data management and, perhaps, wireless transmission. A complete SHM system can provide a vast amount of data related to the behavior and performance of bridge structures over the years. In the case of fatigue damage, based on the accumulated data, a SHM system can be used to assess the remaining life of the monitored structure and detect in advance sudden structural anomalies that could lead to severe damage or even collapse. In other cases, the collected data include information on the time, location, and degree of potential structural deterioration, thus allowing a more rational knowledge-based maintenance scheduling that can reduce maintenance costs and extend the life span of the structure.

The short-term solution that will be the focus of this study is a periodic monitoring of bridges with sensors and measurement instruments. When properly installed, the sensors can be used to determine the location and severity of the damage that affects the overall bridge rating. For example, a crack pattern on the surface of a RC structural member (or bridge system) together with the member design can be used to evaluate the flexural capacity of the member using a mechanics-based equation that relates the crack distribution to the stress in reinforcing bars (Greene et al. 2005). Based on the flexural capacity and the truck model, engineers can rate the member or bridge system. Once potential problem areas are identified, visual inspection is still necessary and invaluable to either confirm the problems or find a remedial solution. Equally importantly, the coaxial cable sensing system is cost effective for large-scale structures, rugged in harsh environment, reliable in measurement, and easy to use.

3.1 Electromagnetic Wave-Guide Sensing System

The distributed nature of coaxial cables and the inexpensive measurement instrument afford them wide applications in typical bridge structures. Cable sensors still gave meaningful signals even after concrete specimens tested in the laboratory completely collapsed. They have a unique "memory" feature, which allows engineers to record potential damage during or immediately after an extreme event such as blasts and earthquakes. The proposed sensor and instrument provide user-friendly images that can be taken by engineers to directly pinpoint the location and severity of damage as discussed in Fig. 1.
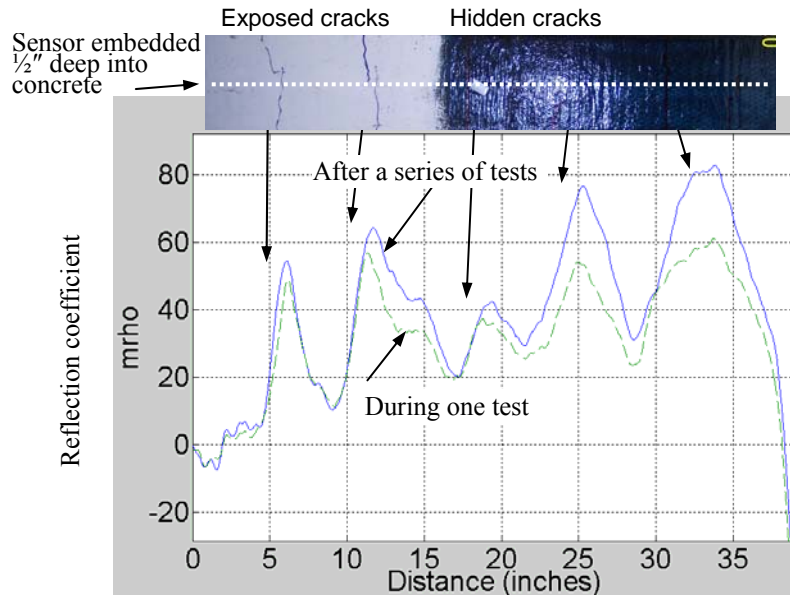
Fig. 1 Two Measurements during and after Shake Table Tests

The proposed sensor and instrument are basically a communication coaxial cable and a fast ETDR system as illustrated in Figs. 2(a, b). A communication coaxial cable consists of a solid inner conductor, a cylindrical outer conductor, and a cylindrical dielectric layer in between the conductors. The outer conductor of a coaxial cable sensor for distributed crack detection is spirally wrapped around the dielectric layer so that the finished outer conductor is mechanically in spiral shape but electrically cylindrical. To ensure the continuity between spirals at zero strain, outside the outer conductor is a thin layer of plasma sprayed coating (Brower et al. 2006). When a crack sensor is embedded into a RC member, a crack intercepting the sensor creates a local separation between two spirals, generating a reflected electromagnetic wave when traveling through the coaxial cable, an electromagnetic wave guide.

3
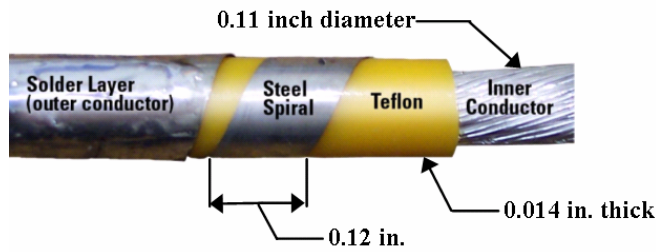
(a) Prototype coaxial cable sensor   (b) Fast ETDR instrument

Fig. 2 Distributed Cable Sensor and Sensing System

A commercial ETDR system consists of a pulse generator and an oscilloscope. The pulse generator with a time-domain reflectometer (TDR) sampling head launches a step pulse (incident wave) with a fast-rising edge (20 or 30 nanoseconds) into a coaxial cable, also called the transmission line, as schematically shown in Fig. 3(a). The oscilloscope monitors and displays both the incident voltage wave (the step pulse generated) and the reflected voltage wave from any disturbed point along the cable since the current flow path on the outer conductor of the cable has been altered as illustrated in Fig. 3(b). When the incident pulse encounters a discontinuity (due to cracking) at any point of the transmission line, a portion of the wave is reflected back as shown in Fig. 3(a). The arrival time of the reflected wave provides the information of the distance between the discontinuity and the monitoring point (at the TDR sampling head), and the amplitude of the reflected wave stands for the degree of the discontinuity. As such, a coaxial cable sensor can be used to detect both the spatial distribution/location and severity of cracks.
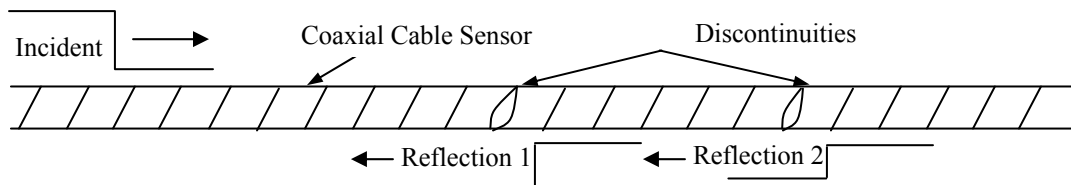
(a) Wave propagation and reflection at discontinuities
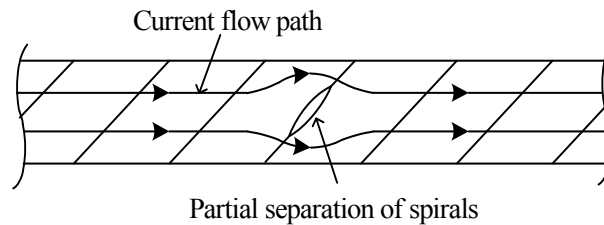
(b) Change in current flow path

Fig. 3 Schematic View of Sensor Working Principle

However, a commercial ETDR cannot be applied for real-time monitoring or any high frequency signal measurements, such as the opening and closing process of an earthquake-induced crack. It takes a relatively long time (seconds) to record one crack distribution profile at any time instance

from triggering an ETDR system to capturing and saving one combined incident and reflected wave on the oscilloscope.

The fast ETDR system, Fig. 2(b), mainly consists of a fast pulse generator, a directional coupler, a combiner, a compensation circuit, and a TDS7404 oscilloscope. It allows for a sequence of crack distribution profiles placed one after another into memory without saving them until completion of the measurements. As such, retriggering delays of microseconds can be achieved. To improve the dynamic range and precision of measurements, unlike any commercial EDTR system, a directional coupler was designed to separate the reflected wave from the incident wave, both traveling through a coaxial cable sensor. Furthermore, a compensation circuit was introduced to cancel out part of the reflected wave that is independent of the crack-induced signal along the cable sensor, representing the effect of mismatched characteristic impedances between the cable sensor and the extension cable.

3.2   Distributed Optical Fiber Sensing System

Alternative solutions for the condition-based inspection of deteriorating structures include the use of optical fibers and Brillouin Optical Time Domain Reflectometry (BOTDR) system for strain measurements. BOTDR is based on the propagation of a train of incident light pulses and Brillouin back-scattering transmitted through an optical fiber. It has been one of the most practical approaches for distributed strain sensing (Gu et al. 2000, Bao et al. 2001, Horiguchi et al. 1989, Ishii et al. 2002, Kaurashima and Sato 1997, Wu et al. 2000, Wu et al. 2002, Wu and Xu 2002). The principle of the operation of an existing backscatter distributed fiber sensing system of BOTDR is similar to that of the optical time domain reflectometer (OTDR). In an OTDR system, a short pulse of light is transmitted along the fiber and the backscattered energy due to Rayleigh scattering is measured at the sending end of the fiber. The time interval between sending the pulse and detection of the backscattering energy provides the spatial information, while the intensity of the backscattered energy provides a measure of the fiber attenuation.

In a BOTDR system, the Rayleigh backscatter mechanism is replaced by Brillouin backscattering. The Brillouin scattered light occurs by an interaction between a high-coherence incident light and an acoustic wave generated by the incident light in an optical fiber. The scattered Brillouin light frequency is shifted from incident light frequency due to the velocity of the acoustic wave. The Brillouin frequency shift is given by the following equation.

$$v_B = 2n v_A / \lambda \tag{1}$$

where n is the refractive index, v_A is the acoustic wave velocity and λ is wavelength of incident light. The frequency shift of Brillouin back-scattering shown in Fig. 4 is a function of both temperature and strain in the fiber. The relationship between strain and frequency shift of Brillouin back-scattering is shown in Fig. 5. The relationship between the Brillouin frequency shift and the tensile strain on the optic fiber can be described by the following equation,

$$v_B(\varepsilon) = v_B(0)(1 + C \cdot \varepsilon) \tag{2}$$

where $v_B(\varepsilon)$ is the Brillouin frequency shift with a strain ε, $v_B(0)$ is the Brillouin frequency shift without a strain, C is the strain coefficient and ε is the strain applied on the fiber.
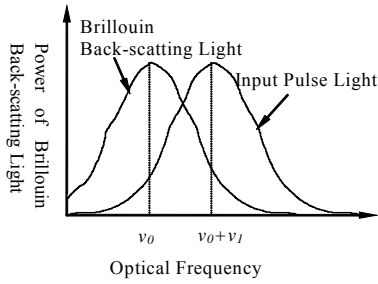
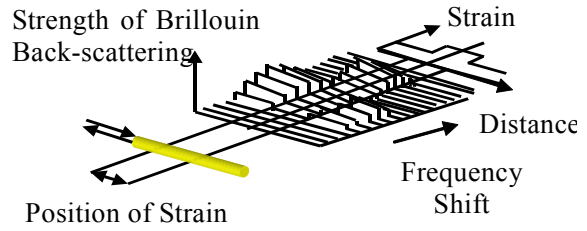Fig. 4 Frequency Shift of Brillouin Back-Scattering

Fig. 5 Relationship between Strain and Frequency Shift of Brillouin Back-Scattering

A strain/loss analyzer AQ8603 (Ando Electric Co. Ltd.) based on the BOTDR technique will be used for the continuous measurement of strain distribution with an optic fiber. Through detecting the amount of the frequency shift of Brillouin back-scattering due to the deformation of the optic fiber, the strain distribution can be measured continuously. According to the principle of BOTDR, the strain at a certain point of measurement is calculated based on the frequency shift of Brillouin back-scattering pulse within its spatial resolution, 3 feet and 8 inches, beyond the point. For a continuous measurement in this study, the measurement interval of sampling points is four inches.

3.3   Comparison between the Two Distributed Sensing Systems

Based on a comparative study by Chen et al. (2005b), the performance comparison between BOTDR and ETDR can be made as summarized in Table 1. During the experiments, it was observed that it took seconds to record the readings from a cable sensor while it took approximately seven minutes to complete one recording using BOTDR. Therefore, ETDR is applicable to both dynamic and static measurements, and BOTDR is for static measurements only. ETDR is sensitive to local deformation such as a crack while BOTDR is not so because of the averaging effect. In addition, optic fibers are much more brittle than coaxial cables for crack detection. On the other hand, optic signal loss in a fiber is extremely low compared to the electrical signal loss in a cable. Thus, over a long distance up to 60 miles, BOTDR can be used for remote monitoring (Nikles et al. 2005), while ETDR can be used for strain measurements in a range of about 100 ft (Sun et al. 2004).

Table 1 Performance Comparison between ETDR and BOTDR

Sensing Property	ETDR	BOTDR
Sensitivity	38~190 mrho/0.01cm crack 13~55 mrho/0.1% strain	500 MHz/% strain
Dynamic measurement	Yes	No
Static measurement	Yes	Yes
Maximum distance	100 ft	60 miles
Spatial resolution	2 in	3 ft
Strain measurement accuracy	± 0.01%	± 0.01%

4   FIELD TEST DESIGN OF A DECOMMISIONED BRIDGE IN JAMESTOWN, NY

In order to validate the performance of coaxial cable sensors and sensing system in field conditions, the North-South Arterial Washington Street Bridge in Jamestown, NY, was identified as an ideal test bed for the proposed technology. The bridge was built around 1962 and is scheduled to be decommissioned in the near future. It is a nine-span simply-supported steel girder structure with drop-in constructions. Each span has five steel girders of 9 ft apart. For easy access during the Phase II field tests in the future, Piers 6-8 and Span 9 were selected for analysis in this Phase I study. Fig. 6 shows the plan view of the bridge with the highlighted area of study.
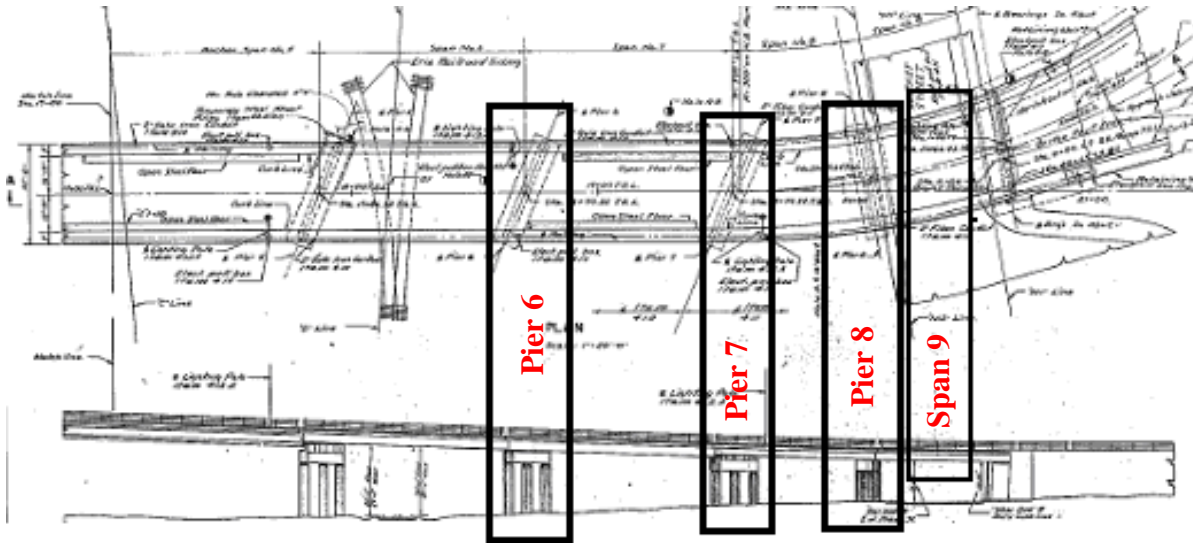
Fig. 6 Plan View of the Jamestown Bridge

Following is a detailed presentation of the predicted deck and pier performance of various tests that are envisioned to take place on the decommissioned bridge. Considering load requirements for the full-scale bridge in field conditions, only members and components will be considered to be tested to various failure modes.

4.1   Test Design of Pier 6

4.1.1 Field test setup

Pier 6 consists of a RC capbeam and three RC columns. As illustrated in Fig. 7, the pier will be tested under a concentrated load applied at the middle height of two adjacent columns in one bay. To ensure that the other bay of the three-column pier remains steady during the field tests, a steel bracing may be considered to stiffen the reaction system. It is expected that the actual load will be applied on an $18" \times 24"$ area by a load apparatus, which is 11.0 ft above the bottom of the column. The detailed design of the loading apparatus is also illustrated in Fig. 7. Starting from one end, the apparatus consists of an attachment plate on the RC column, a steel rod roller, a steel plate connected to one end of the hydraulic actuator, the actuator, a load cell connected to the other end of the actuator, an extension steel rod welded to an end steel plate, another steel rod

roller and an attachment steel plate. Both the load cell and extension steel rod are placed inside a steel tube that prevents the potential buckling of the test apparatus under a compressive load.
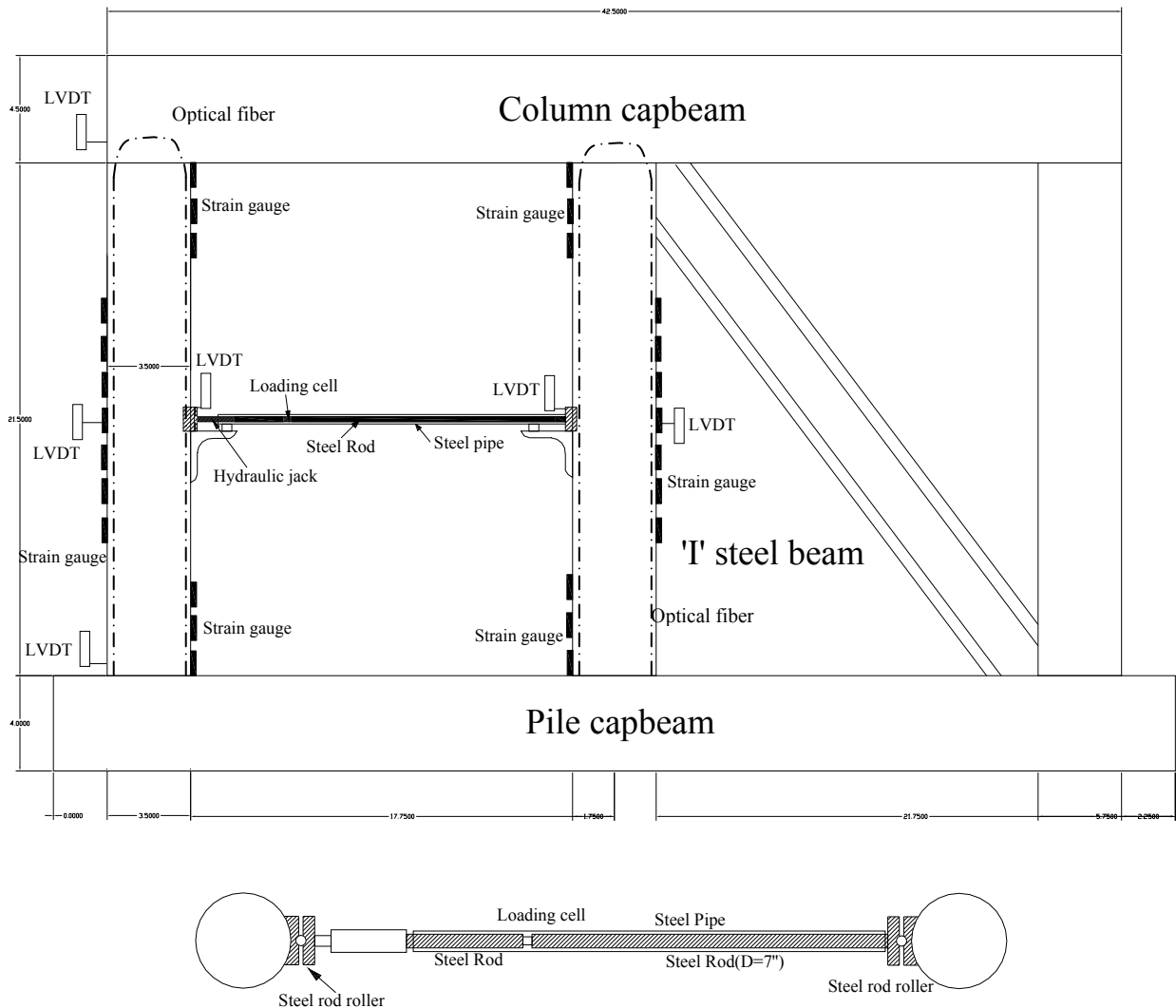
Fig. 7 Test Setup of Pier 6

Pier 6 will be instrumented with six Linear Voltage Differential Transformer (LVDT) units for deflection measurements, 26 strain gauges for strain measurements along the concrete surface, a BOTDR optical fiber system for strain and temperature measurement, and an ETDR coaxial cable sensing system for crack detection. It is envisioned that three data acquisition systems will be used to record deflection and strain from LVDTs and strain gauges, strain and temperature from the BOTDR optical fiber, and crack from the ETDR system.

4.1.2 FEM of a column

A finite element model (FEM) of a RC column was established in DIANA software to simulate the load test process in field condition. As illustrated in Fig. 8, this model simulates concrete and

8

steel reinforcement separately. The concrete part is modeled with eight-node solid elements and the steel reinforcing bar is simulated with rebar elements that behave like truss members. The FEM has a total of 4830 nodes with each node having three translational motions, at both end of the column there are 150 nodes without any movement to simulate fixed end, so totaling 13,590 degrees.

The Grade 60 steel reinforcement used in the column design has a Young's modulus of $E_s =$ 30,000,000 psi and yield strength of $f_s = 60,000$ psi. The concrete has a Young's modulus of $E_c =$ 3,600,000 psi, tensile strength of $f_t = 423\,psi$, compressive strength of $f_c = 4000\,psi$, and fracture energy of $G_f^I = 2.5\,lbf\,/\,in$. As shown in Fig. 9, the exponential softening model and the Thorenfeldt model were used to model the tensile and compressive behaviors of the concrete.

(a) Concrete model (b) Steel model	
Fig. 8 FEM of the Column at Pier 6	Fig. 9 Stress-Strain Curve of Concrete
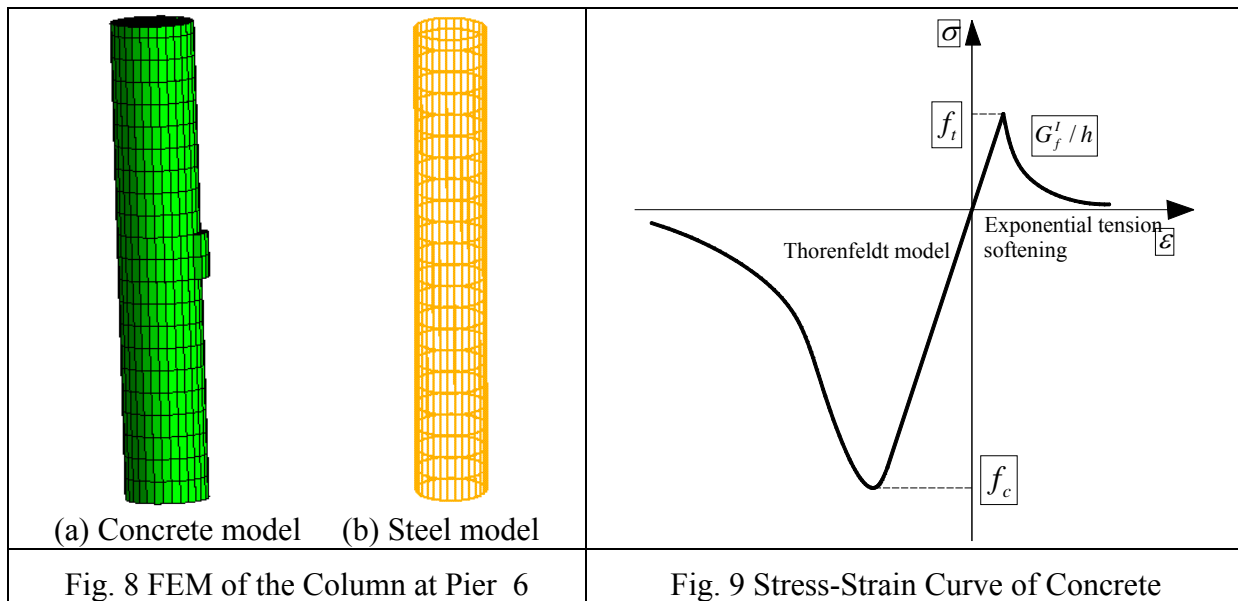
4.1.3 Results and discussions

For each analysis, a total of 79 loading steps was applied to Pier 6 in displacement control. The load-displacement curve is presented in Fig. 10. It consists of an initial concrete crack, elastic steel deformation, steel yielding, and collapse. The maximum load that can result in the column collapse is 1360 kips at a displacement of approximately 0.33 inches. Note that steel yielding corresponds to a mid-height column displacement of approximately 0.26 inches.
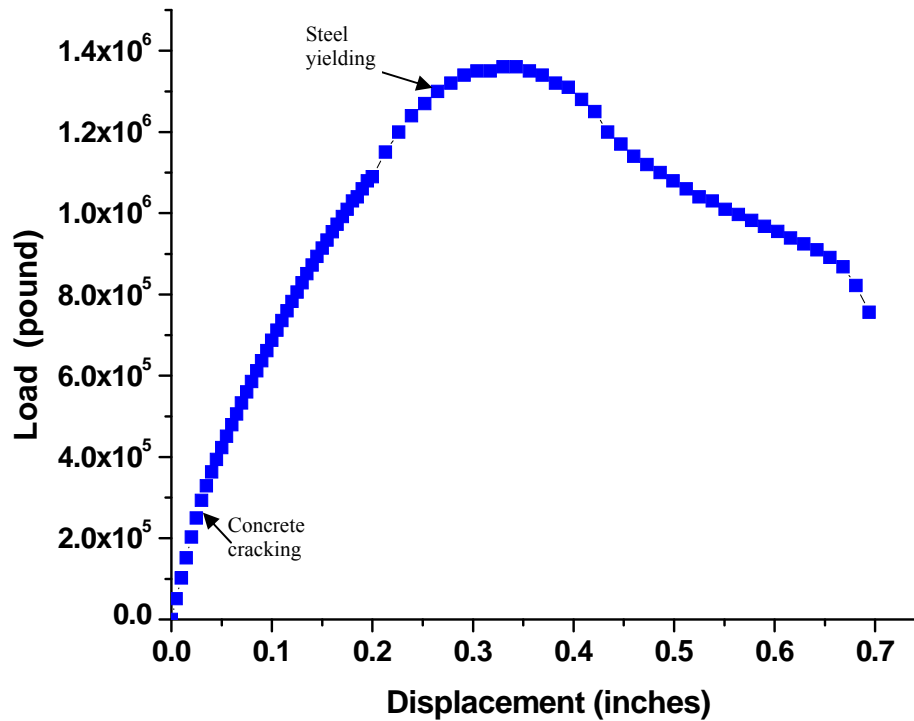
Fig. 10 Load-Displacement Curve of the Column at Pier 6

The stress and crack distributions under various loads are presented in Fig. 11. It can be clearly seen from Fig. 11(a) that the stress was concentrated at the two ends and the mid-height of the column. As a result, cracks develop at these locations as illustrated in Fig. 11(b).

As the cracks at both ends of the column fully penetrates the cross section, two plastic hinges form as shown in Figure 11(b). As the crack in the mid-height of the column fully penetrates its cross section under a load of 1360kips, the column collapses due to steel yielding at both ends and the mid-height of the column.
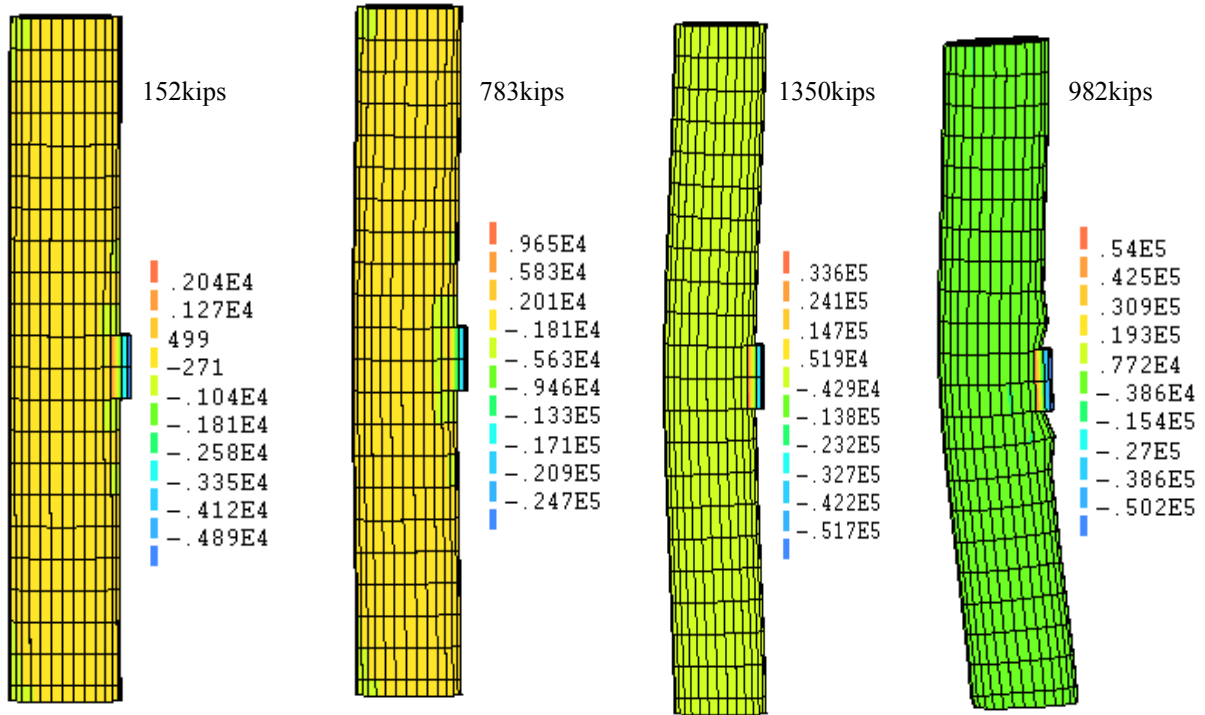
(a) Stress distribution under various loads
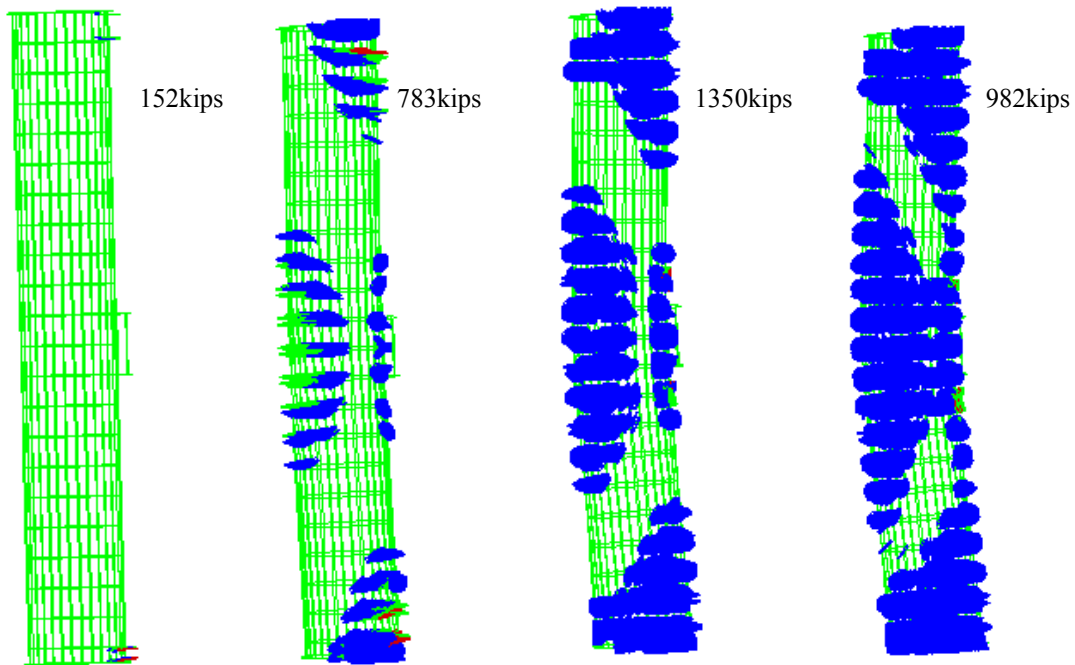
(b) Crack distribution

Fig. 11 Stress and Crack Distributions under Various Loads

To understand the onset of flexure and shear cracks, the detailed crack distributions at two ends and mid-height of the column were investigated. As presented in Fig. 12, the first flexural crack

appears at both ends of the column under a load of 152 kips (shown by straight lines perpendicular to the column axis in Fig. 12). Both shear cracks and flexural cracks develop with the increase the load (shown by horizontal and inclined lines in Fig. 12, respectively). At the ultimate load of 1360 kips, the flexural and shear cracks are shown in Fig. 13. Both the ends and mid-height are close to experience fully penetrated cracks.

(a) Flexural cracks at end under 152kips   (b) Flexural cracks at mid-height under 783kips

(c) Shear cracks at end under 783kips   (d) Shear cracks at mid-height under 1350kips
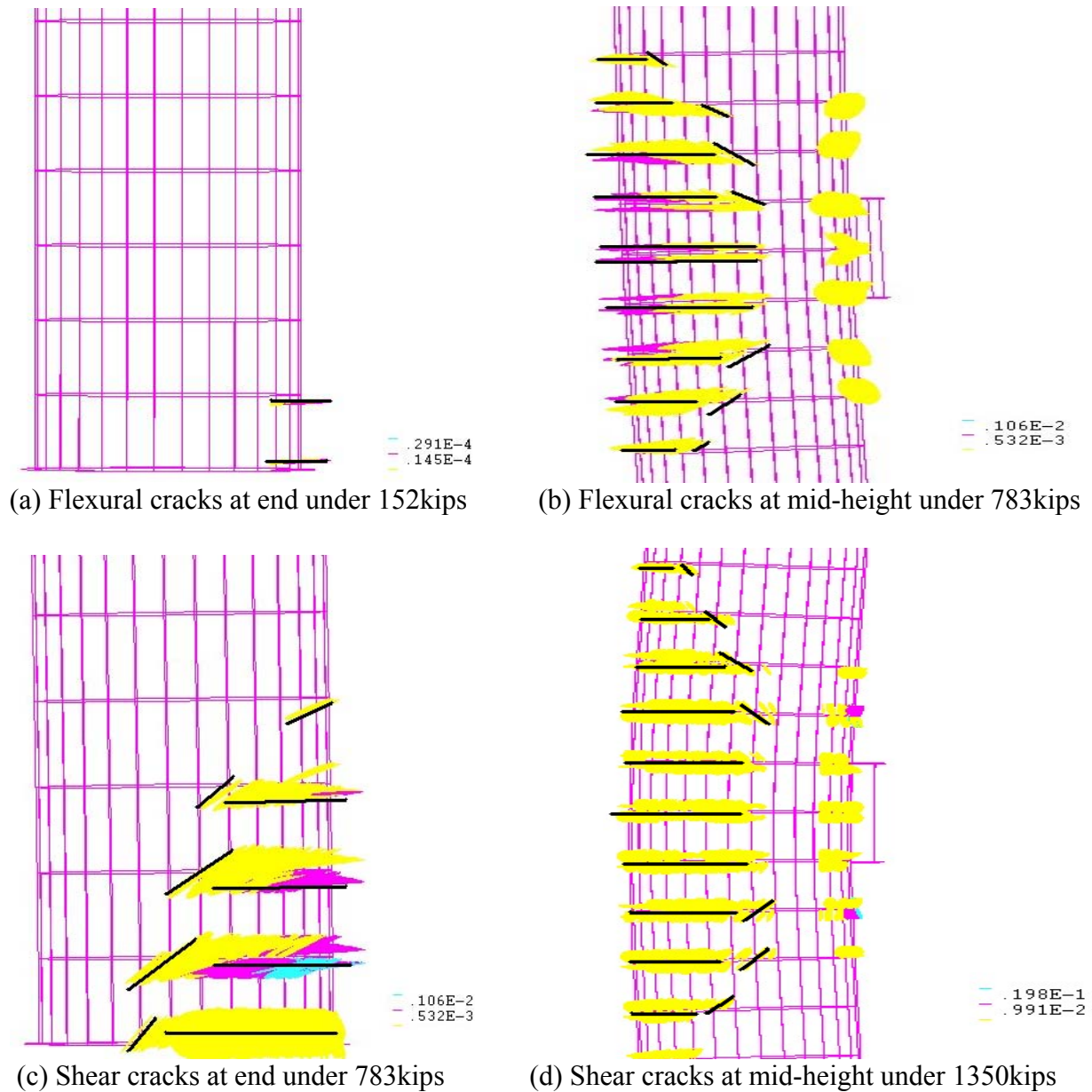
Fig. 12 Onset of Flexural and Shear Cracks on the RC Column under Various Loads
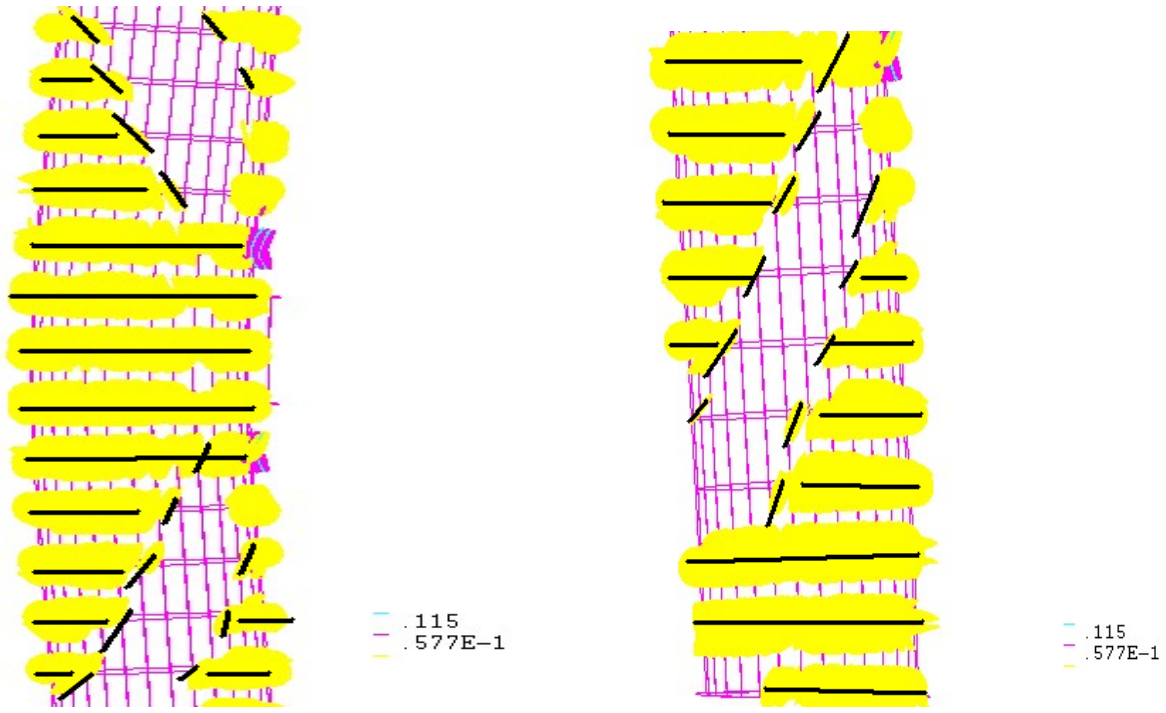
(a) Mid-height of the column   (b)   End of the column

Fig. 13 Flexural and Shear Crack Distributions at the Ultimate Load of 1360 kips

The stress distribution along the steel reinforcement near and far sides of the loading point is presented in Fig. 14. On the near side, the main reinforcement is subjected to compression at mid-height of the column and tension at both ends of the column. It can be clearly observed from Fig. 14 that at 1350 kips, all steel reinforcing bars on the loading side yield at both ends and the mid-height of the column. On the far side, the mid-span tensile bars appear to experience more yielding.
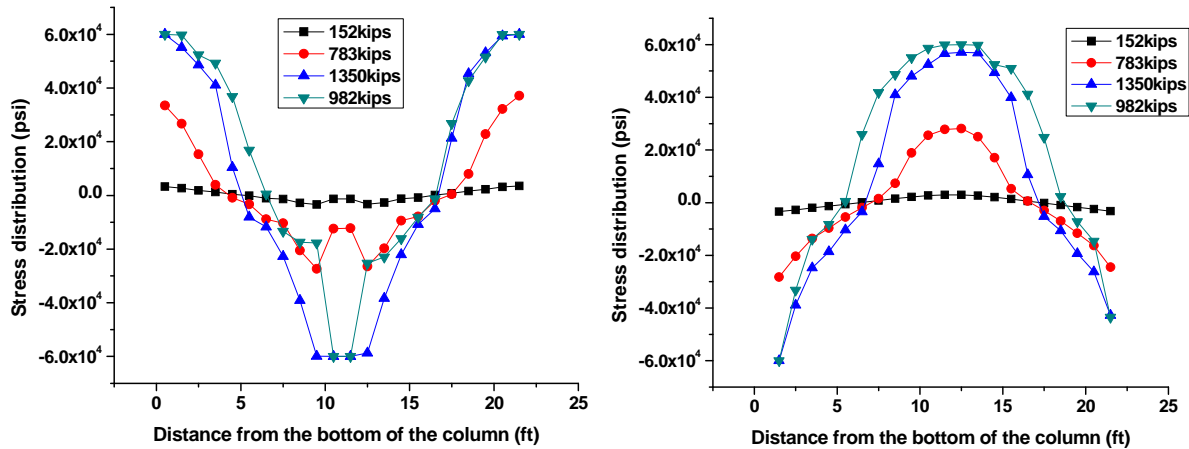
(a) Near side of the loading region   (b) Far side of the loading region

Fig. 14 Stress Distribution in Main Steel Reinforcement of the Column

13

4.1.4 Summary on Pier 6 performance

Based on the above numerical analyses, the following observations can be made:
- (1) The first flexural crack appears at the two ends of the column under a load of approximately 260 kips.
- (2) The column would form a collapsible mechanism at a load of 1360 kips when the far side reinforcement of the loading point and near side of both ends and the loading point experienced yielding simultaneously. The column fails due to steel yielding.

4.2   Test Design of Pier 7

4.2.1 Field test setup

Similar to Pier 6, Pier 7 consists of a RC capbeam and three RC columns. It will be tested as illustrated in Fig. 15 under a concentrated load applied at the mid-height of two adjacent columns in one bay. It is expected that the actual load was applied on an $15" \times 24"$ area by a load apparatus, which is 8 ft above the bottom of the column. The detailed design of the loading apparatus is identical to that illustrated in Fig. 7. Pier 7 will be instrumented with six LVDT units for deflection measurements, 22 strain gauges for strain measurements along the concrete surface, a BOTDR optical fiber system for strain and temperature measurement, and an ETDR coaxial cable sensing system for crack detection.

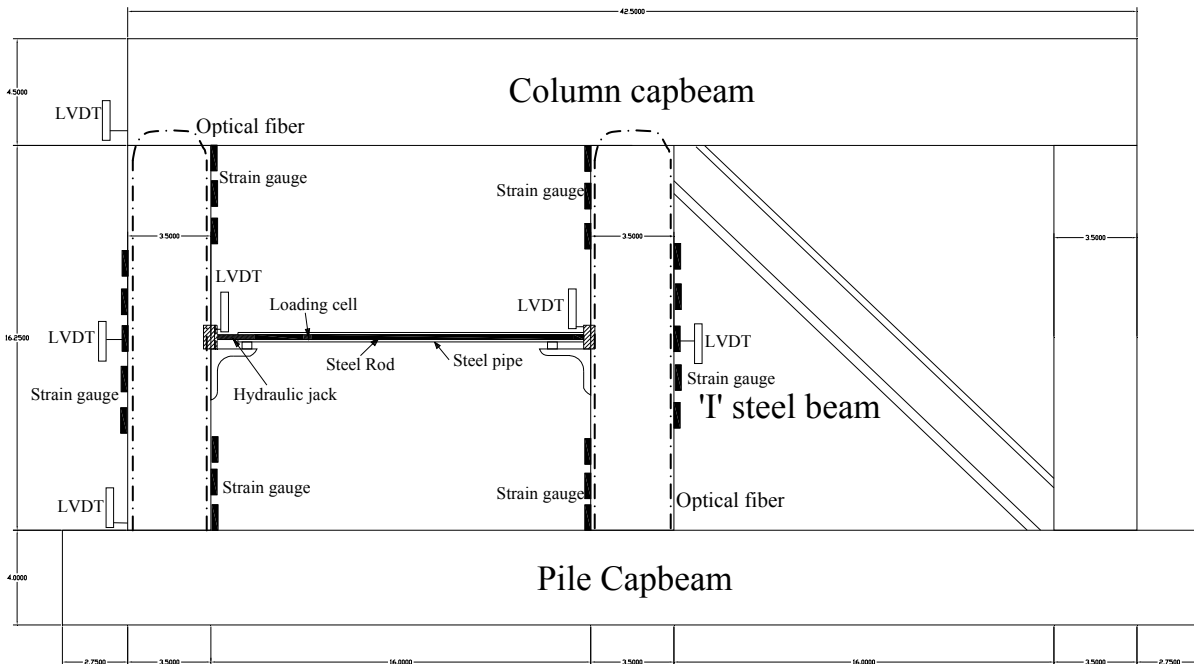Fig. 15 Test Setup of Pier 7

4.2.2 Results and discussions

A FEM similar to Fig. 8 was established in DIANA software for the column in Pier 7 to be tested. The same material and material models were considered in numerical analysis. The load-

displacement curve is presented in Fig. 16. It consists of an initial concrete crack, elastic steel deformation, steel yielding, and collapse. The maximum load that can result in the column collapse is 1440 kips at a displacement of approximately 0.28 inches.
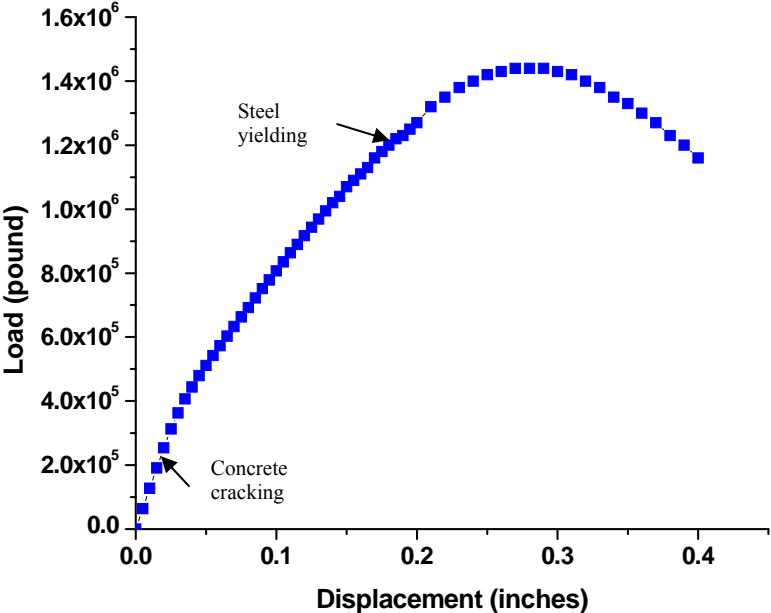
Fig. 16 Load-Displacement Curve of the Column at Pier 7

The stress and crack distributions under various loads are presented in Fig. 17. It can be clearly seen from Fig. 17(a) that the stress was concentrated at the two ends and the mid-height of the column. As a result, cracks develop at these locations as illustrated in Fig. 17(b).

As the crack at both ends of the column penetrates the cross section, two plastic hinges forms under a load of approximately 1250kips. When the crack in the mid-height of the column fully penetrates its cross section, the column reaches its ultimate load 1440kips. The column fails due to steel yielding at both ends and the mid-height.
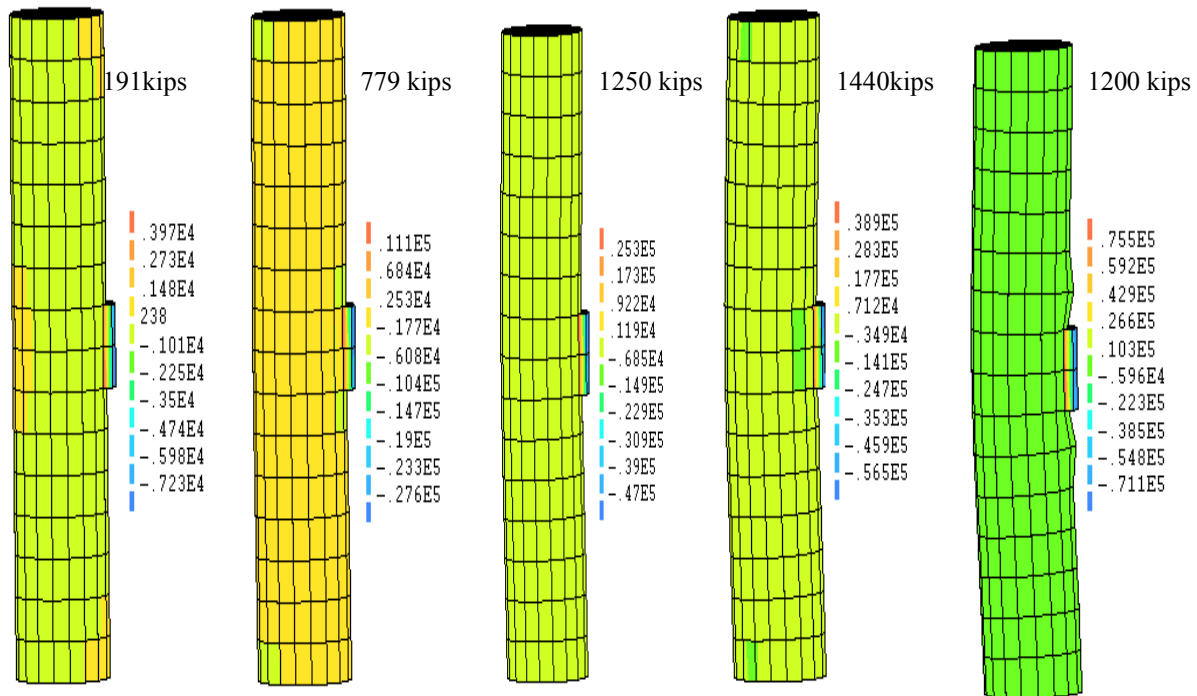
(a) Stress distribution under various loads
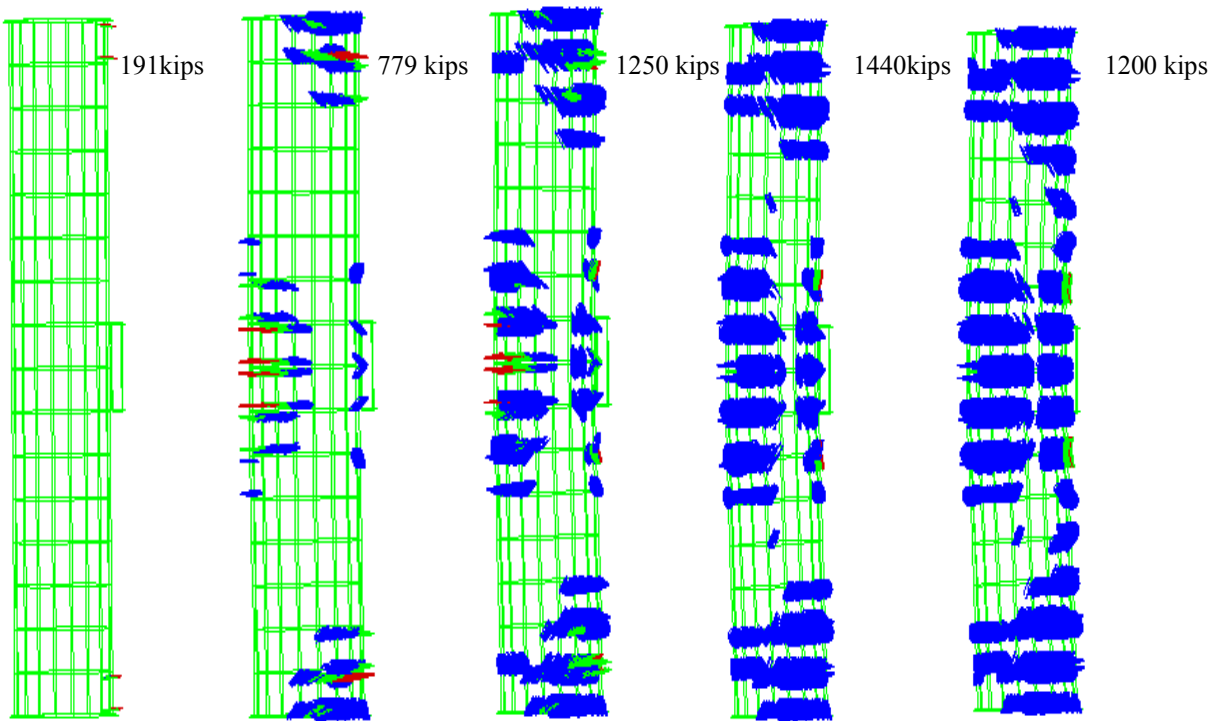
(b) Crack distribution

Fig. 17 Stress and Crack Distributions under Various Loads

To understand the onset of flexure and shear cracks, the detailed crack distributions at two ends and mid-height of the column were investigated. As presented in Fig. 18, the first flexural crack

appears at its ends under a load of 191 kips (shown by straight lines perpendicular to the column axis in Fig. 18). Both shear cracks and flexural cracks develop with the increase of load (shown by inclined lines and straight lines to the column axis in Fig. 18). At the ultimate load of 1440 kips, the flexural and shear cracks are shown in Fig. 19. Both the ends and the mid-height are close to experience fully penetrated cracks.
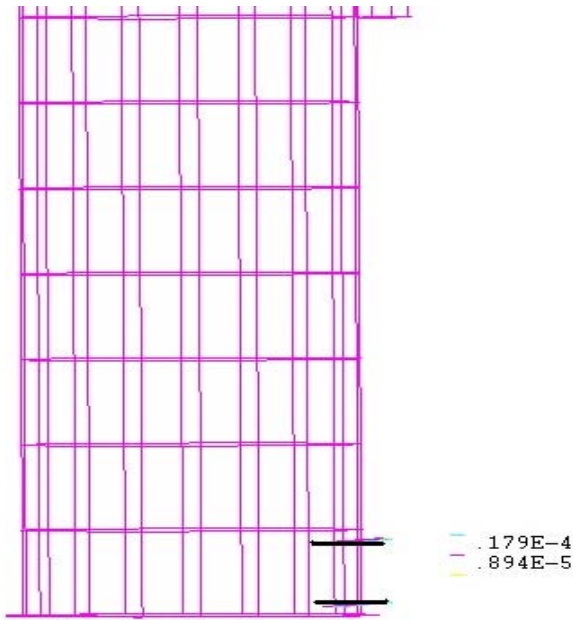
(a) Flexural cracks at end under 191kips
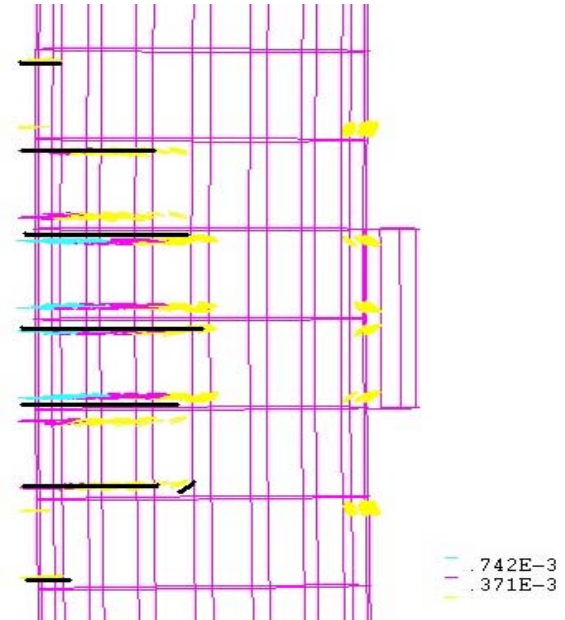
(b) Flexural cracks at mid-height under 779kips
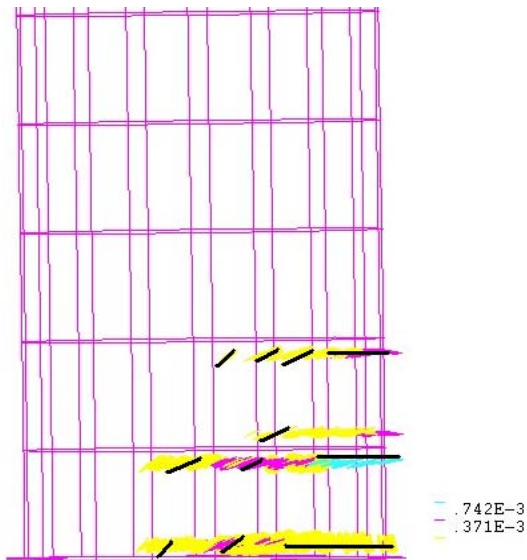
(c) Shear cracks at end under 779kips
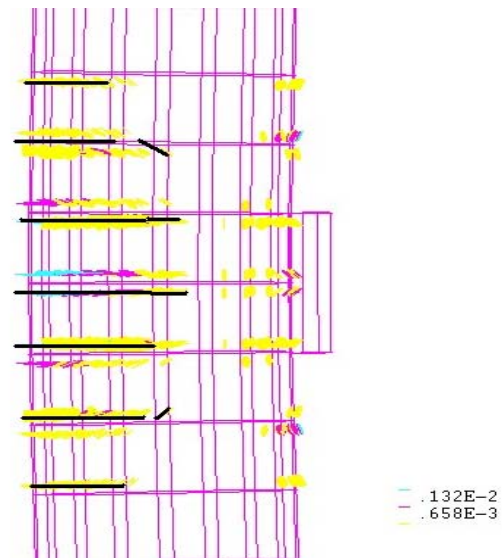
(d) Shear cracks at mid-height under 1250kips

Fig. 18 Onset of Flexural and Shear Cracks on the RC Column under Various Loads

(a) Mid-height of the column   (b)   End of the column
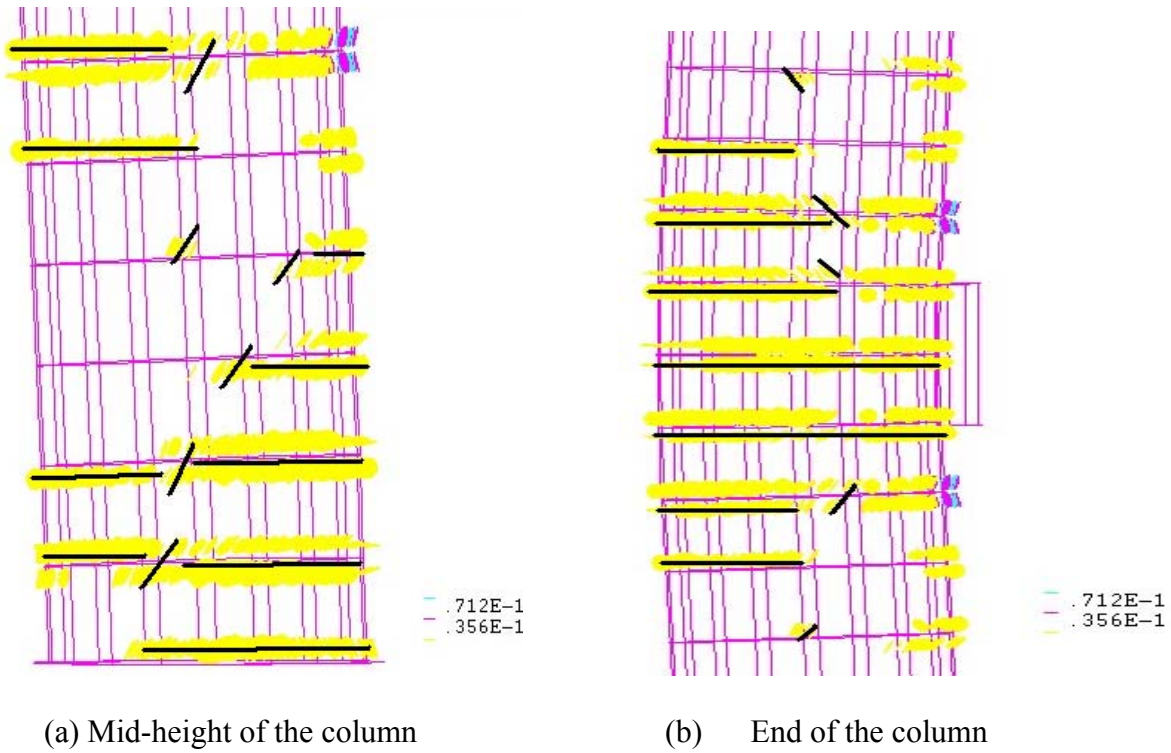
Fig. 19 Flexural and shear crack distributions at the ultimate load of 1440 kips

The stress distribution along the steel reinforcement near and far sides of the loading point is presented in Fig. 20. On the near side, the main reinforcement is subjected to compression at mid-height of the column and tension at both ends of the column. It can be clearly observed from Fig. 20 that at both ends and the mid-height of the column, all steel reinforcing bars yield under an ultimate load of 1440 kips.

(a) Near side of the loading region   (b) Far side of the loading region
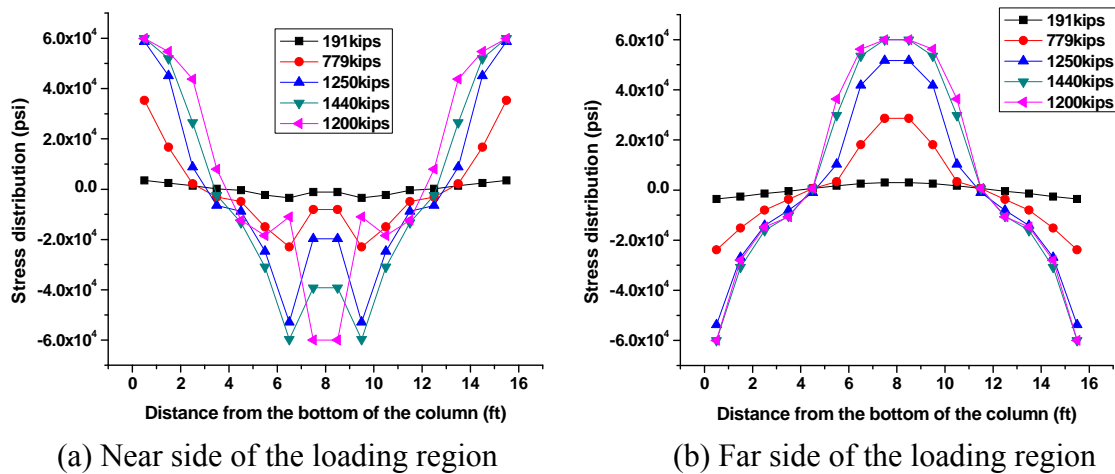
Fig. 20 Stress Distribution in Main Steel Reinforcement of the Column

18

4.2.3 Summary on Pier 7 performance

Based on the above numerical analyses, the following observations can be made:
  (1) The first flexural crack appears at the mid-height and both ends of the column under a load of approximately 250 kips.
  (2) The column would form a collapsible mechanism at a load of 1440 kips when the far side reinforcement of the loading point and near side of both ends experienced yielding simultaneously. The column fails due to steel yielding.

4.3   Test Design of Pier 8

4.3.1 Field test setup

Similar to Pier 6 and 7, Pier 8 consists of a RC capbeam and three RC columns. It will be tested under a concentrated load applied at the middle height of two adjacent columns in one bay as illustrated in Fig. 21. It is expected that the actual load was applied on an $15" \times 24"$ area by a load apparatus, which is 7 ft above the bottom of the column. The detailed design of the loading apparatus is identical to that illustrated in Fig. 7. Pier 8 will be instrumented with six LVDT units for deflection measurements, 22 strain gauges for strain measurements along the concrete surface, a BOTDR optical fiber system for strain and temperature measurement, and an ETDR coaxial cable sensing system for crack detection.
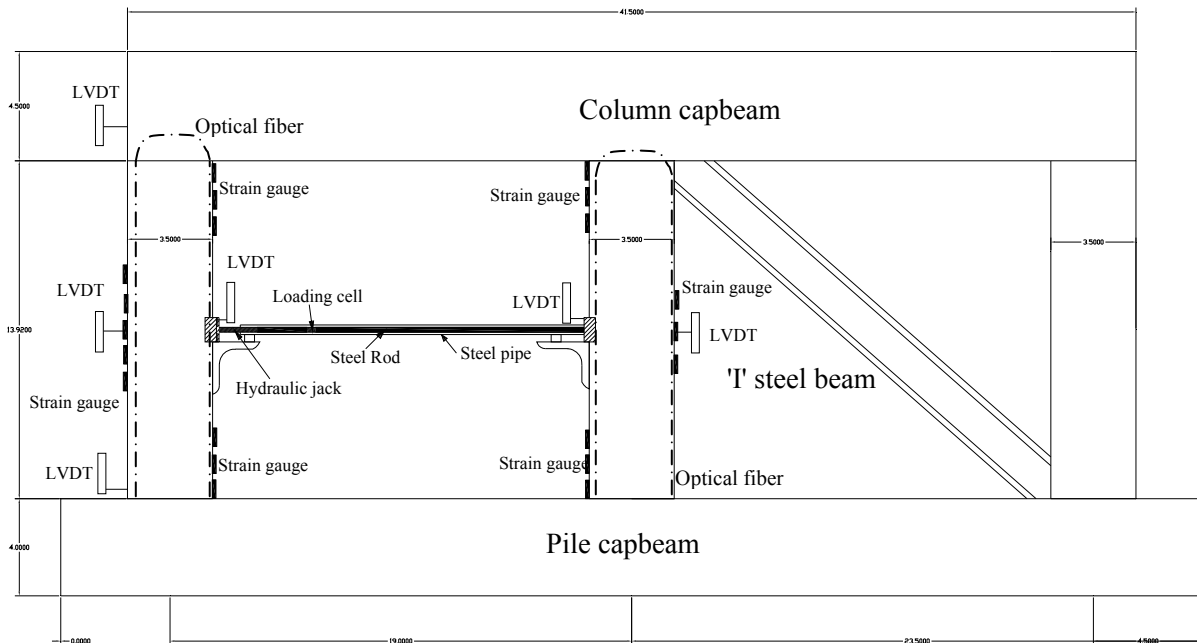
Fig. 21 Test Setup of Pier 8

4.3.2 Results and discussions

A FEM similar to Fig. 8 was established in DIANA software for a column in Pier 8. The same material and material models were considered in numerical analysis. The load-displacement curve is presented in Fig. 22. It consists of an initial concrete crack, elastic steel deformation,

steel yielding and collapse. The maximum load that can result in the column collapse is 1440 kips at a displacement of approximately 0.18 inches.
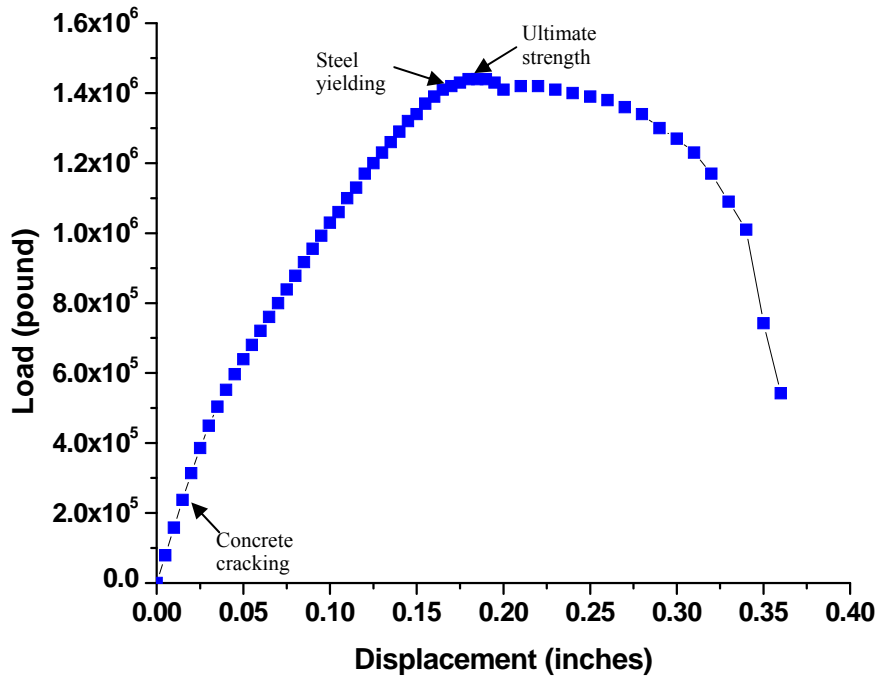
Fig. 22 Load-Displacement Curve of the Column at Pier 8

The stress and crack distributions under various loads are presented in Fig. 23. It can be clearly seen from Fig. 23(a) that the stress was concentrated at the two ends and the mid-height of the column. As a result, cracks develop at these locations as illustrated in Fig. 23(b).

In the beginning of loading, the flexural cracks develop at both ends and the mid-height of the column. With the increase of load, the shear crack develops as shown by inclined lines in Figure 23 (b). When the load reaches 1440 kips, the shear cracks intersect with flexural cracks at both ends, the cracks penetrates the cross section of the column.
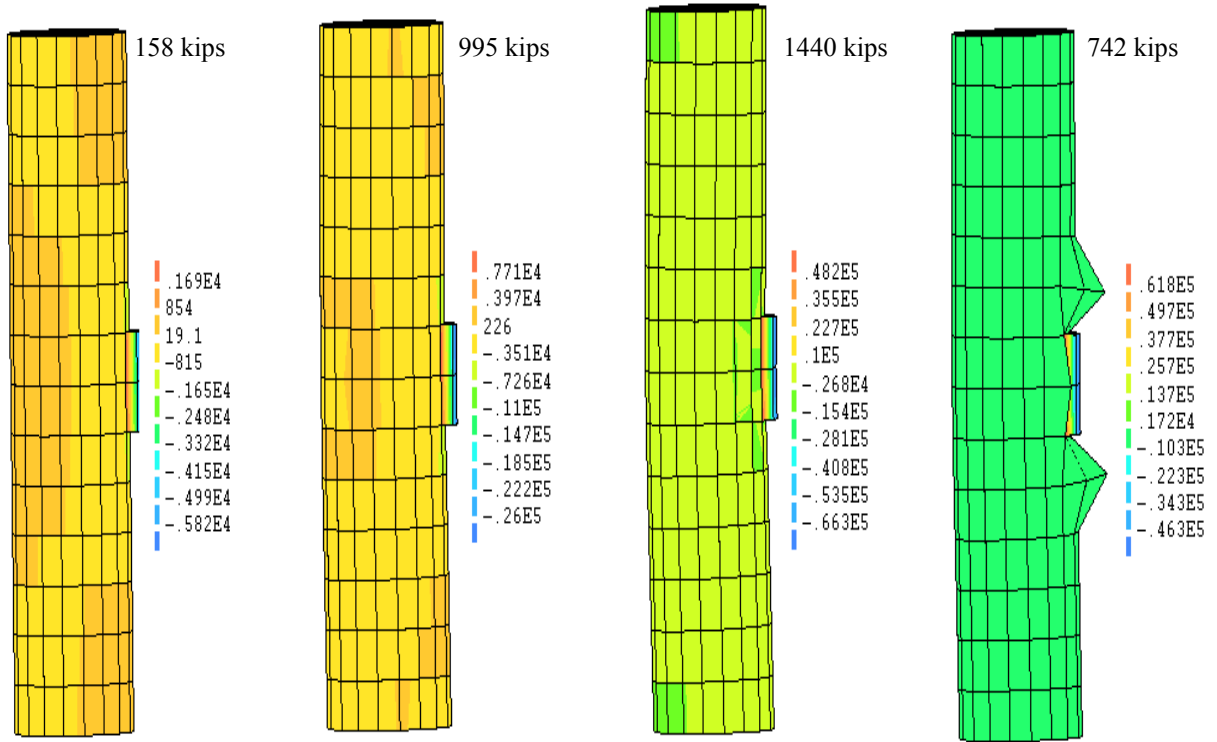
(a) Stress distribution under various loads
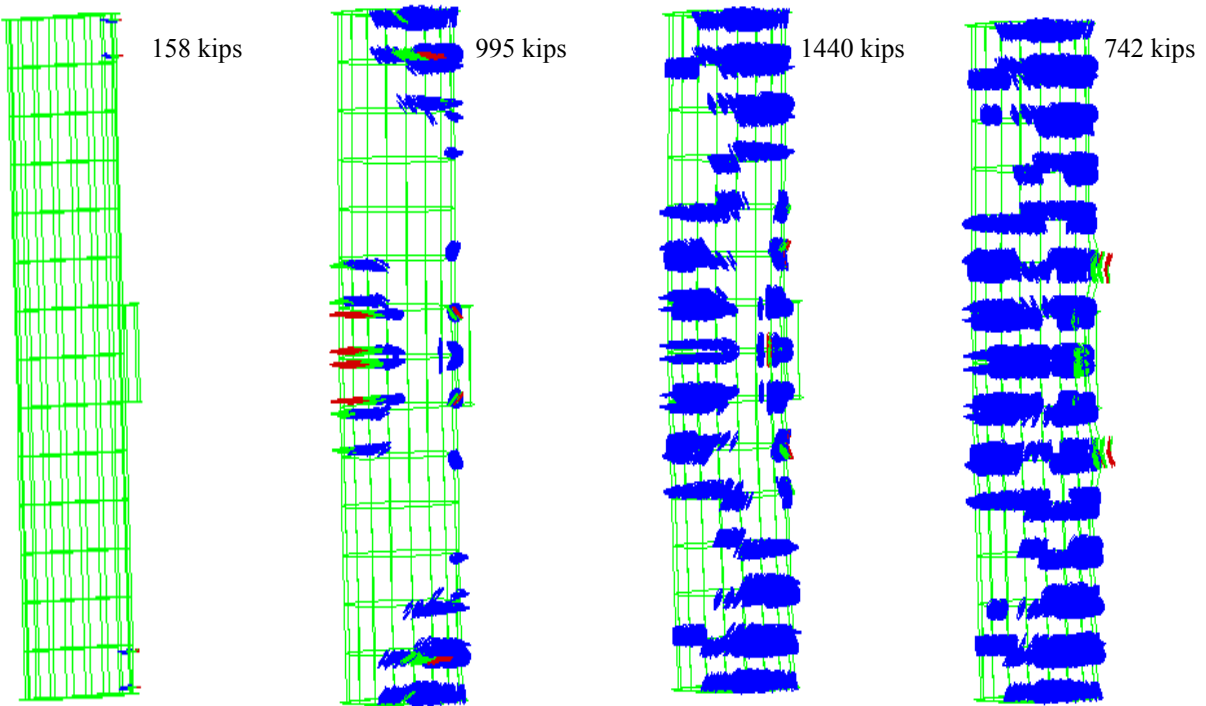
(b) Crack distribution

Fig. 23 Stress and Crack Distributions under Various Loads

To understand the onset of flexure and shear cracks, the detailed crack distributions at two ends and mid-height of the column were investigated. As presented in Fig. 24, the first flexural crack appears at its ends under a load of 158 kips (shown by straight lines perpendicular to the column axis in Fig. 24). Both shear cracks and flexural cracks develop with the increase of load (shown by inclined lines and straight lines to the column axis in Fig. 24). At the ultimate load of 1440 kips, the flexural and shear cracks are shown in Fig. 25. Unlike piers 6 and 7, just the ends of the column at pier 8 experienced full penetration of cracks.
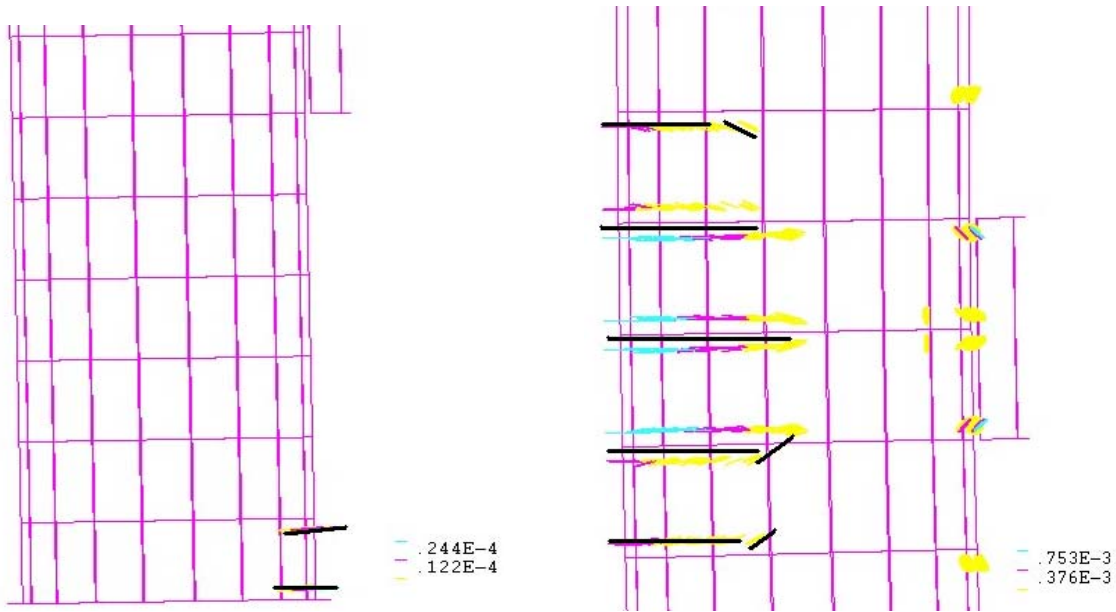
(a) Flexural cracks at end under 158kips (b) Flexural cracks at mid-height under 995kips
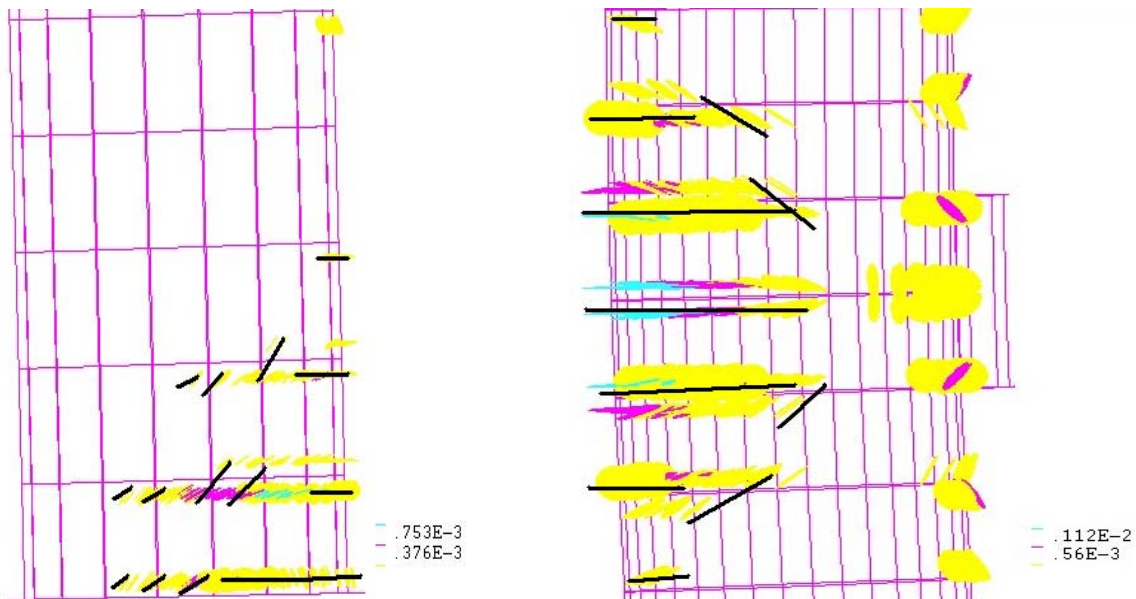
(c) Shear cracks at end under 995kips   (d) Shear cracks at mid-height under 1290kips

Fig. 24 Onset of Flexural and Shear Cracks on the RC Column under Various Loads

22
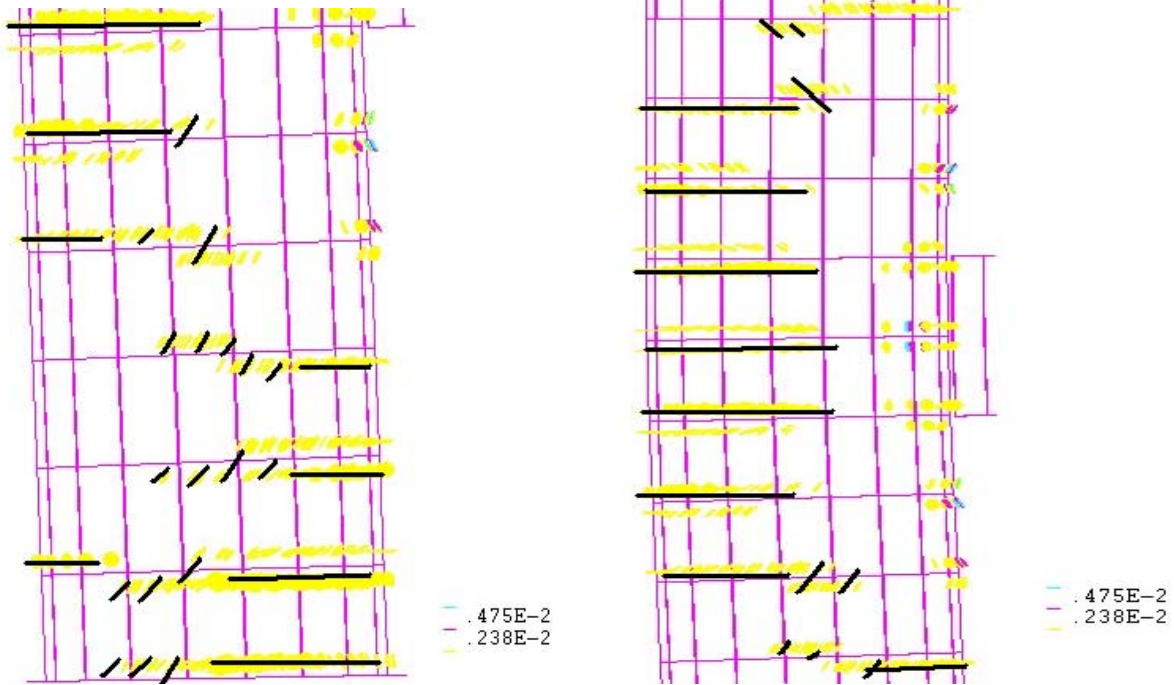
(a) Mid-height of the column   (b)   End of the column

Fig. 25 Flexural and Shear Crack Distributions at the Ultimate Load of 1440 kips

The stress distribution along the steel reinforcement near and far sides of the loading point is presented in Fig. 26. The main reinforcing bars on both sides are subjected to a similar magnitude of compressive and tensile stresses at the mid-height and both ends of the column. It can be clearly observed from Fig. 26 that only at both ends of the column, the steel reinforcing bars yield when the load reaches ultimate load 1440kips.
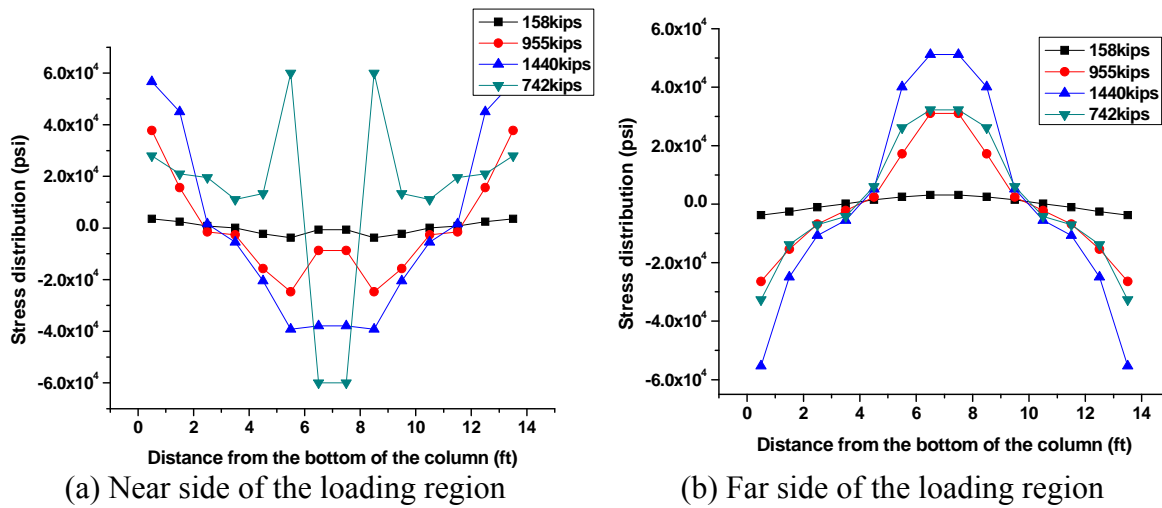
(a) Near side of the loading region   (b) Far side of the loading region

Fig. 26 Stress Distribution in Main Steel Reinforcement of the Column

23

4.3.3 Summary on Pier 8 performance

Based on the above numerical analyses, the following observations can be made:
  (1) The first flexural crack appears at the mid-height and both ends of the column under a load of approximately 240 kips.
  (2) The column would fail in both flexure and shear at a load of 1440 kips. The steel only at both ends of the column reaches yielding under ultimate load.

4.4   Test Design of a Simply-Supported Bridge Deck in Span 9

4.4.1 Field test setup

The first deck of 3'-9" wide will be cut out of Span 9 of the decommissioned bridge along the transverse direction between two adjacent girders. As illustrated in Fig. 27, the deck is 9' long (steel girder spacing) and simply supported at both ends on the steel girders. The deck will be tested under a steel plate with dimensions $45"\times 6"\times 2"$ applied at the mid-span of the deck.
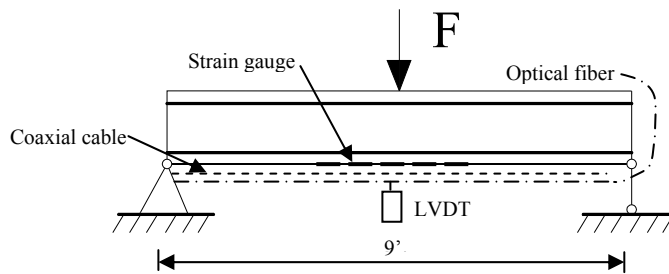
Fig. 27 Test Setup of the First Deck

The simply-supported deck will be instrumented with two LVDT units for deflection measurements, five strain gauges for strain measurements along the concrete surface, a BOTDR optical fiber system for strain and temperature measurement, and an ETDR coaxial cable sensing system for crack detection. It is envisioned that three data acquisition systems will be used to record deflection and strain from LVDTs and strain gauges, strain and temperature from the BOTDR optical fiber, and crack from the ETDR system.

4.4.2 FEM of the simply-supported deck

A FEM of the RC deck was established in DIANA software to simulate the load test process in field condition. As illustrated in Fig. 28, this model simulates concrete and Grade 60 steel reinforcement separately. The concrete part is modeled with eight-node solid elements and the steel reinforcing bar is simulated with rebar elements that mimic the behavior of a truss system. The FEM has a total of 635 nodes with each node having three translational degrees. Seven nodes at the left end are pin supported, and seven nodes at the right end are restrained in vertical direction only. The model has a total of 1876 degrees. The same material properties as used for Piers 6 - 8 were considered for the deck analysis. The concrete stress-strain curve is shown in Fig. 9.
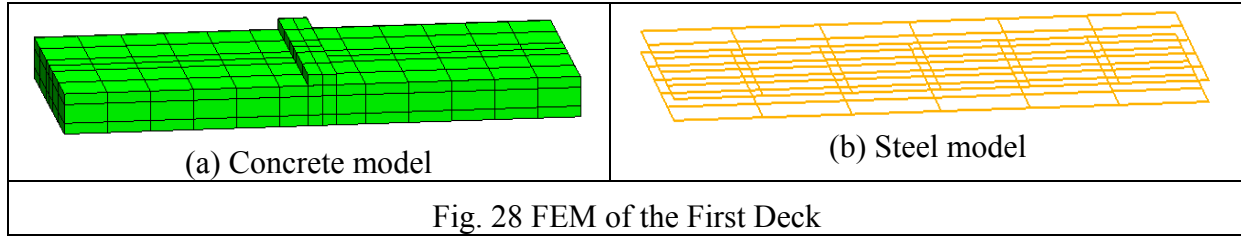
(a) Concrete model	(b) Steel model
Fig. 28 FEM of the First Deck	

4.4.3 Results and discussions

During the numerical analysis, a total of 150 loading steps were applied to the simply-supported deck in displacement control. The load-displacement curve is presented in Fig. 29. It consists of an initial concrete crack, elastic steel deformation, steel yielding, and collapse. The maximum load that can result in the deck collapse is approximately 17 kips at a displacement of approximately 1.0 inches. Note that steel yielding corresponds to a mid-span displacement of approximately 0.60 inches.
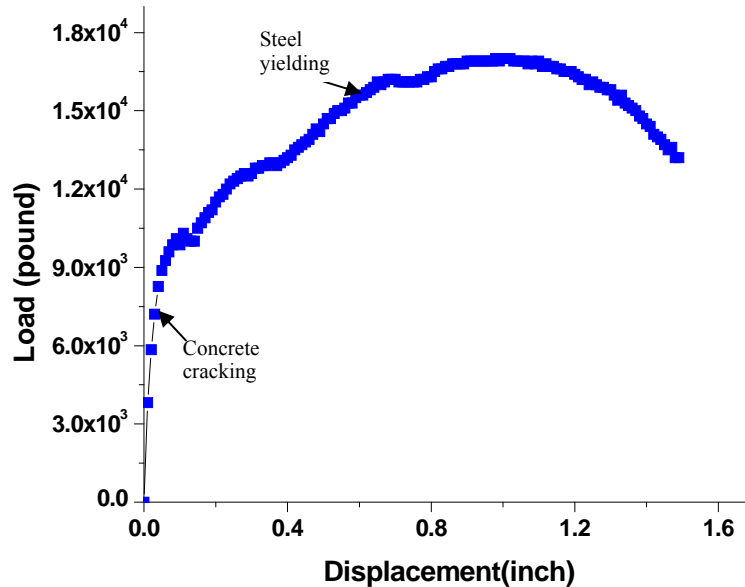
Fig. 29 Load-Displacement Curve of the Simply-Supported Deck

The stress and crack distributions under various loads are presented in Fig. 30. It can be clearly seen from Fig. 30(a) that the stress was concentrated at the mid-span of the deck. As a result, cracks develop at this location as illustrated in Fig. 30(b).

As the crack at mid-span of the deck fully penetrates its cross section, the strain in reinforcement continues to increase, exhibiting a significant amount of inelastic deformation as evidenced in Fig. 31. Fig. 30 also supports the observation with no clear indication of concrete crushing.

25
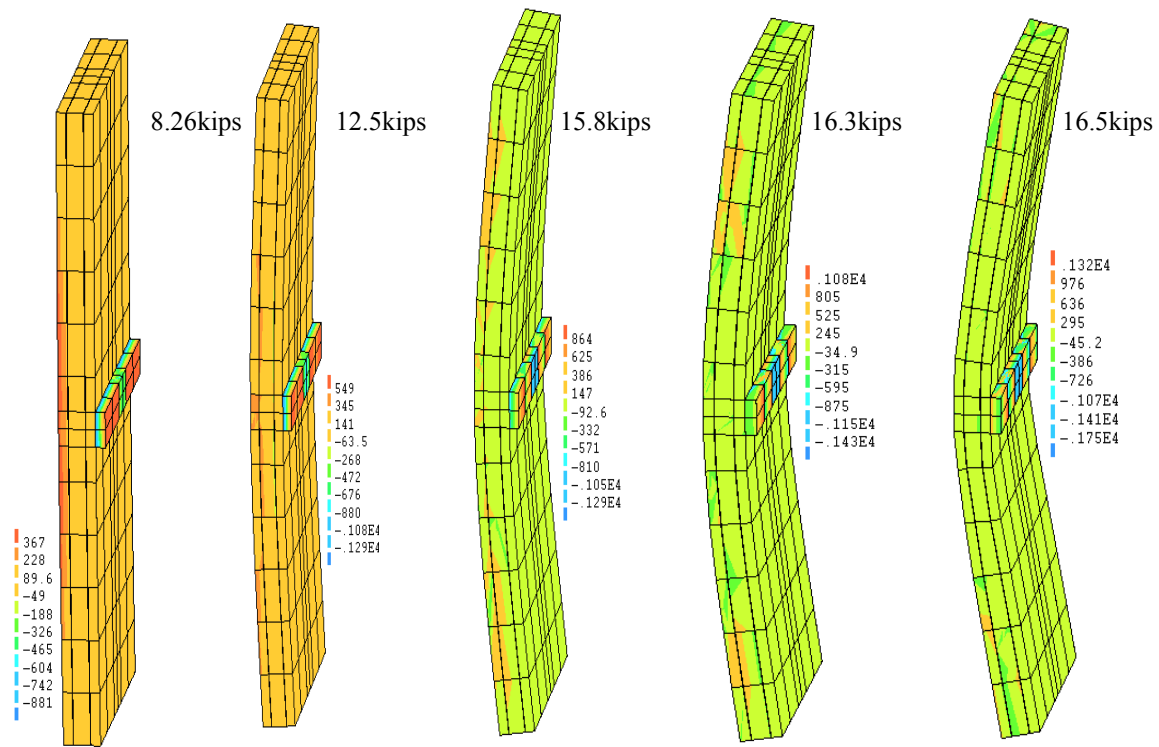
(a) Stress distribution under various steps of loading
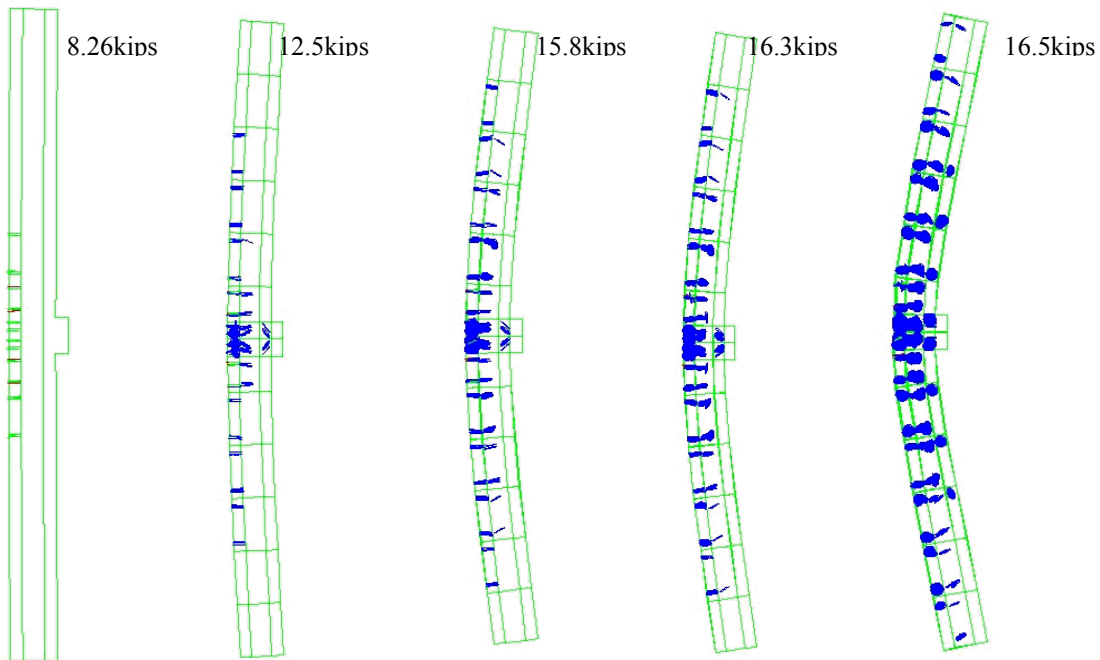
(b) Crack distribution

Fig. 30 Stress and Crack Distributions under Various Steps of Loads

The stress distribution along the main steel reinforcement on the top and bottom of the deck is presented in Fig. 31. The main reinforcement is mainly subjected to compression on the top reinforcement and tension on the bottom reinforcement of the deck. It can be clearly observed

from Fig. 31 that both the top and the bottom steel in the middle of the deck reach yielding under an ultimate load of approximately 16.5 kips, forming a plastic hinge at mid-span.

(a) Top reinforcement   (b) Bottom reinforcement
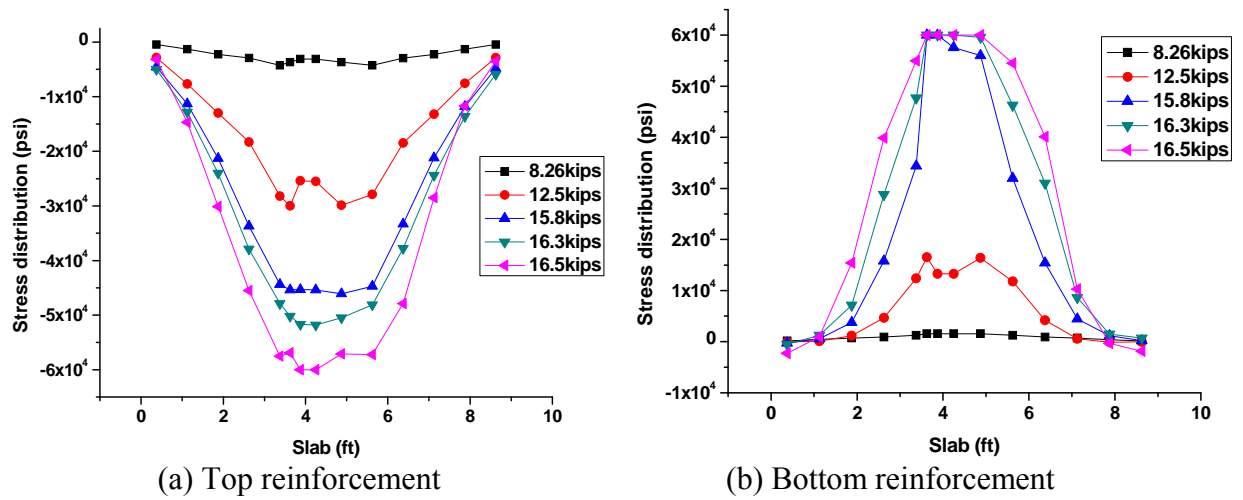
Fig. 31 Stress Distribution in Main Steel Reinforcement of the Deck

4.4.4 Summary on the simply-supported deck performance

Based on the above numerical analyses, the following observations can be made:
(1) The first flexural crack appears at a load of approximately 7.5 kips.
(2) The bottom and the top reinforcement reached yielding at a load of 16.50 kips at a mid-span deflection of 0.6 inches. The ultimate load of the deck is 17 kips.

4.5   Test Design of a Two-Span Continuous Deck

4.5.1 Field test setup

The second deck of 3'-9" wide will be cut from Span 9 of the decommissioned bridge along the transverse direction between two adjacent girders. As illustrated in Fig. 32, the two-span deck of 9' long each is a continuous slab. The deck will be tested under two steel plates with dimensions $45" \times 6" \times 2"$ applied at the mid-spans of the two spans.
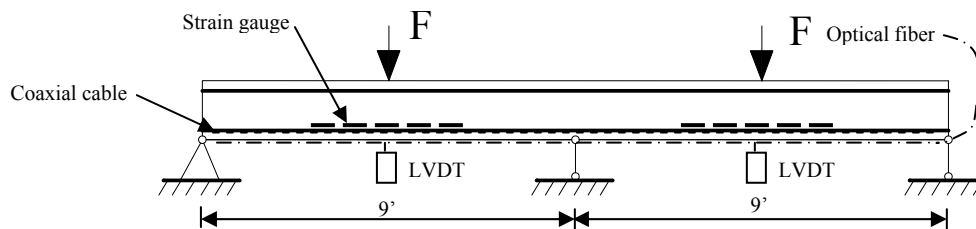
Fig. 32 Test Setup of the Two-Span Continuous Deck

The continuous deck will be instrumented with four LVDT units for deflection measurements, 10 strain gauges for strain measurements along the concrete surface, a BOTDR optical fiber system for strain and temperature measurement, and an ETDR coaxial cable sensing system for crack

detection. Like the simply-supported deck, three data acquisition systems will be used to record deflection and strain from LVDTs and strain gauges, strain and temperature from the BOTDR optical fiber, and crack from the ETDR system.

4.5.2 Results and discussions

A FEM of the continuous deck similar to Fig. 28 was established in DIANA software. For each test, a total of 100 loading steps will be applied to the continuous deck in displacement control. The load-displacement curve is presented in Fig. 33. It consists of an initial concrete crack, elastic steel deformation, steel yielding at different locations, and collapse due to plastic hinges. The maximum load that can result in the deck collapse is approximately 23.7 kips at a displacement of approximately 0.40 inches. Note that steel yielding corresponds to a mid-span displacement of approximately 0.20 inches under a load of 20 kips. After the displacement reaches about 0.5inches, one plastic hinge forms near the fixed end of the deck, so the load decrease rapidly and the displacement continues to increase as shown in the decreasing part of Fig.33.
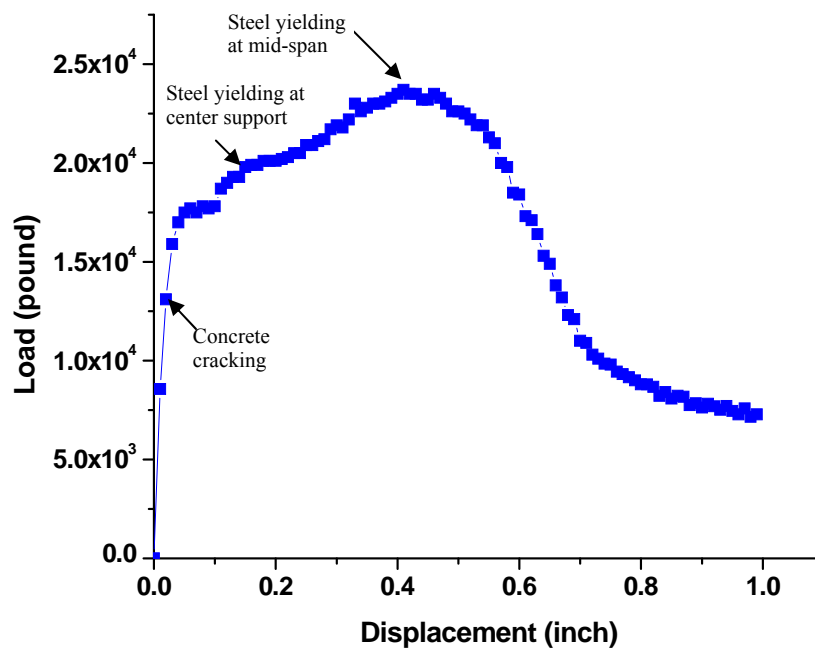
Fig. 33 Load-Displacement Curve of the Continuous Deck

The stress and crack distributions under various loads are presented in Fig. 34. It can be clearly seen from Fig. 34(a) that the stress was concentrated at the mid-span of the deck. As a result, cracks develop at this location as illustrated in Fig. 34(b).
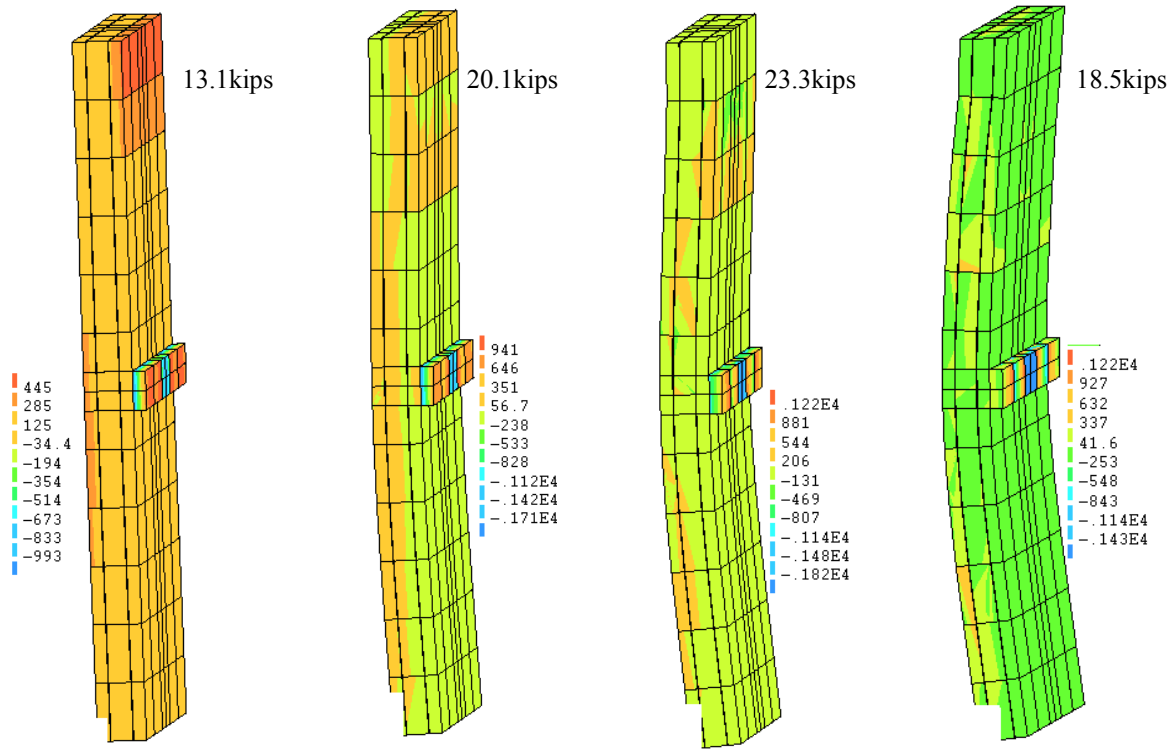
(a) Stress distribution under various steps of loading
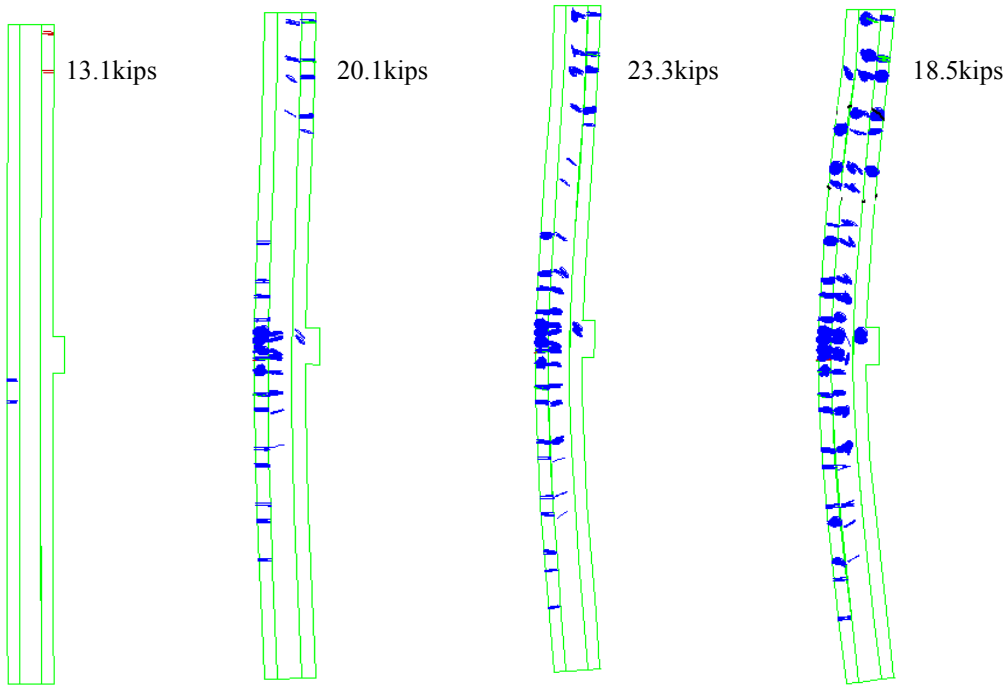
(b) Crack distribution

Fig. 34 Stress and Crack Distributions under Various Steps of Loads

The stress distribution along the main steel reinforcement on the top and bottom of the deck is presented in Fig. 35 for half of the deck span. The main reinforcement is mainly subjected to compression on the top reinforcement and tension on the bottom reinforcement at mid-span of the deck. At the center support, a negative moment was generated, causing tension on the top reinforcement and compression on the bottom reinforcement. It can be clearly observed from Fig. 35 that, at mid-span of the span, the maximum compressive stress is less than the material yield strength but the tensile stress almost reached to the yield strength. At the center support, the top reinforcement almost reaches yielding in tension while the bottom reinforcement experiences compression. Once the mid-span and center support cross section yield simultaneously, a collapsible mechanism will be formed. Note that the crack at mid-span and the part close to the fixed end of the deck fully penetrates its cross section.

(a) Top reinforcement　　　　　　　　(b) Bottom reinforcement
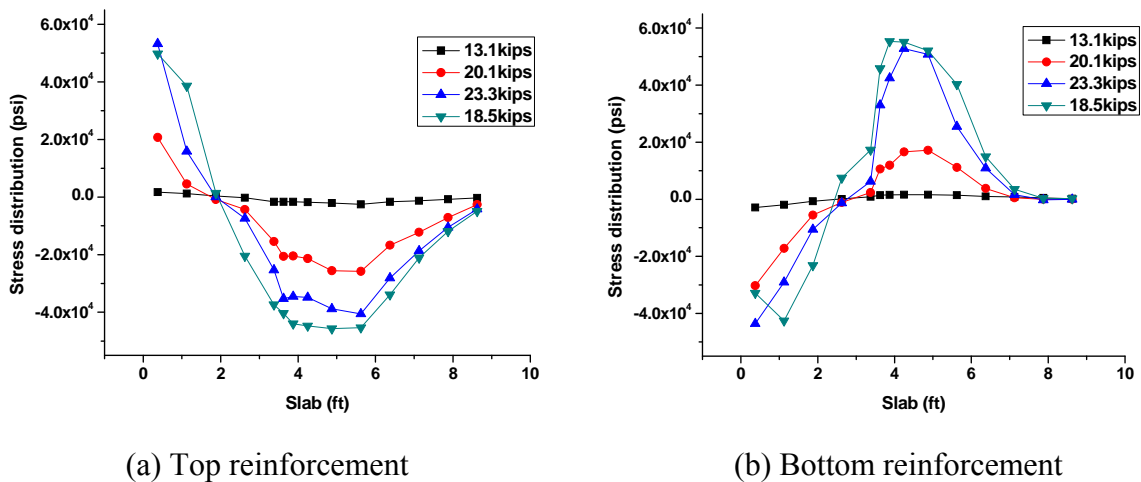
Fig. 35　Stress Distribution in Main Steel Reinforcement of the Deck

4.5.3 Summary on the continuous deck performance

Based on the above numerical analyses, the following observations can be made:
  (1) The first flexural crack appears at a load of approximately 13 kips.
  (2) The top reinforcement at center support will yield first and the bottom reinforcement at mid-span will yield secondly.
  (3) The bottom reinforcement reached yielding at a load of 20 kips, corresponding to a mid-span deflection of 0.2 inches. The ultimate load is 23.7 kips at a mid-span deflection of 0.4 inches.

5　RECOMMENDATIONS ON FIELD TEST PLAN AND SCHEDULE

Based on extensive analysis, the following test plan and schedule are recommended. They will be the key activities in the follow-up Phase II study. The objectives of the Phase II study are to qualify and validate the performance of distributed crack sensors and a fast ETDR instrument to their full potential, and to evaluate the potential market of the new technology in civil infrastructure. Five tasks are designed to accomplish the following scope of work:

- Fabricating coaxial cable sensors and characterizing their sensitivity, spatial resolution, signal loss, and "memory" feature with laboratory tests of scaled beams,
- Designing and packaging a fast ETDR instrument for real-time monitoring, and qualifying its precision, dynamic range, and memory size,
- Installing coaxial cable and other sensors on the select bridge such that the performance of the crack sensors can be adequately quantified with the other instruments,
- Field testing the decommissioned bridge to a critical damage state so that a full range of performance from visually invisible to excessive crack widths can be validated, and
- Preparing technical specifications and validation documentations, and estimating the potential market of coaxial cable sensors in civil infrastructure applications.

Task 1 Test Plan

The bridge deck will be tested in a simply-supported span or two continuous spans. As detailed in Fig. 36, its test setup includes:
- Transversely saw cut the bridge deck (Span 9) into three strips of 3.75 ft each,
- Longitudinally saw cut each strip into one single-span and one two-span slabs,
- Install coaxial cables and other sensors (not shown in Fig. 36 for clarity) for comparison,
- Rest a double-channel reaction beam on the deck with wood pads,
- Insert two Dywidag bars through the center of the reaction beam, the deck, and a double-channel support beam underneath a girder, and
- Set up a hydraulic jack between the deck and the reaction beam.

As each hydraulic jack in Fig. 36 pushes the deck against the reaction beam, the bridge deck is subjected to one point load. In the case of two continuous spans, two point loads are applied to the mid-spans of the two spans.
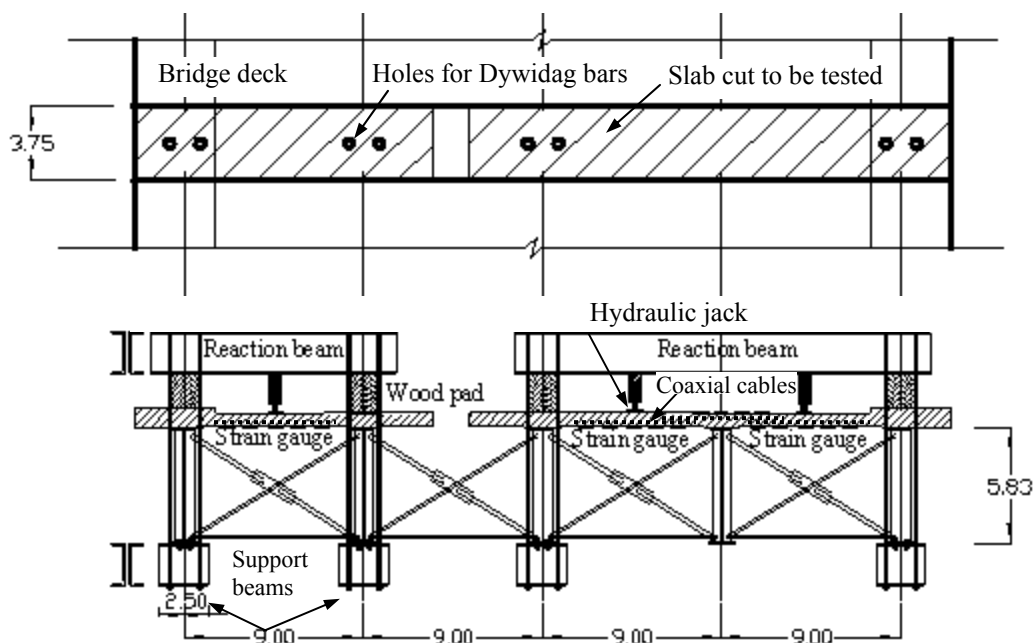

Fig. 36 Test Setup for Bridge Deck (all dimensions in ft)

As detailed in Fig. 37, the bridge column test setup includes:
- Set up a scaffold
- Drill two holes on each column for load plate attachment
- Place a power team cylinder (hydraulic jack) against one column through a load plate
- Place a solid steel rod inside a steel circular tube in alignment with the cylinder
- Apply a preload on the cylinder

As illustrated in Fig. 37, the column will be tested by pushing two columns against each other. To ensure the safety of its supporting bridge deck during field testing, each column is loaded up to 75% of the ultimate load that the column can sustain.
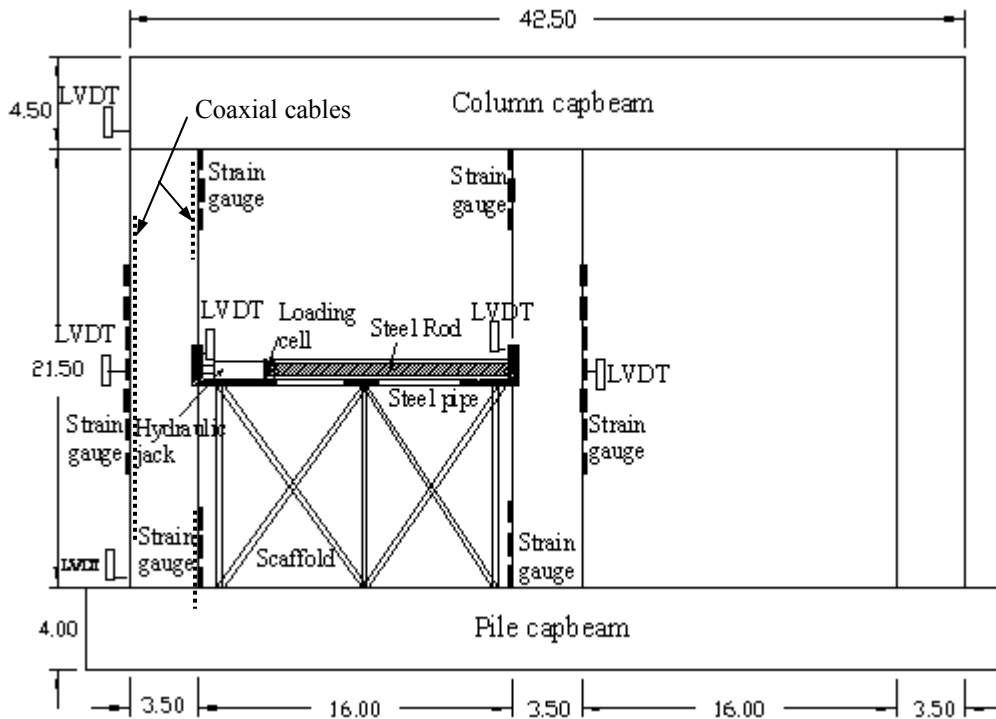
Fig. 37 Test Setup of Bridge Column (all dimensions in ft)

The overall test sequence and duration of the decommissioned bridge is described as follows:
- Test preparation and setup for all columns in Piers 6- 8 (2 months)
- Two columns in Pier 6 loaded to concrete cracking, concrete spalling, and 75% the maximum load corresponding to shear failure (0.75 month),
- Two columns in Pier 7 loaded to concrete cracking, concrete spalling, and 75% the maximum load corresponding to shear failure (0.75 month),
- Test preparation and setup for decks in Span 9 (1 month)
- Three decks in Span 9 loaded to concrete cracking, concrete spalling, initial yielding, and the ultimate strength (0.75 month),
- Two columns in Pier 8 loaded to concrete cracking, concrete spalling, and 75% the maximum load corresponding to shear failure (0.75 month),
- Test site cleanup (0.25 month)

Note that the bridge must be closed during the column and deck tests. However, the column test preparation will be completed before the bridge is decommissioned. To minimize the duration of tests, the deck test preparation will be performed while the columns in Piers 6 and 7 are scheduled to test.

Additionally, to ensure smooth operation at the bridge site, all logistics issues such as electricity, water, and emergency contact plan as well as subcontracting, if required, will be addressed before the test setup begins.

Task 2 Final Design of Field Tests on RC Decks and Columns

Each deck strip will be tested under point loads at mid-span in simply supported or two-span continuous structures. A FEM was developed for each deck strip with 4 ksi concrete and Grade 60 rebar. For the simply-supported slab, concrete cracking occurs at 7.5 kips, the steel rebar yields at 16.5 kips, and the ultimate strength is reached at 17 kips corresponding to 1.0 inch in mid-span. For the two-span continuous slab, concrete cracking occurs at 13 kips, the bottom steel rebar yields at 20 kips, and the ultimate strength is 23.7 kips corresponding to a mid-span deflection of 0.4 inches. These analyses determined the load capacity and stroke requirements of hydraulic jacks for deck testing, which are 50 kips and 2.0 inch.

The columns in Piers 6-8 will be tested with a point load at mid height. Each column was considered to be fixed at both ends. For all columns, the onset of concrete cracking occurs at a load ranging from 240 to 260 kips. The column fails in flexure at a load of 1360 to 1440 kips, corresponding to a stroke of <0.33 inches. As such, the load capacity and stroke requirements for column testing are 1500 kips and 0.5 inches.

The deck and column design will be finalized after the select bridge is decommissioned and material properties of the bridge are obtained from concrete coring and steel sampling.

Task 3 Instrumentation, Field Test and Data Collection

The Center for Infrastructure Engineering Studies (CIES) at Missouri S&T has a 48-channel data acquisition system. Strain gauges will be installed on test structures. Load cell and LVDT will be installed on the test bridge to generate load-displacement curves that provide global damage data for a structural component or system. A cable sensor will be embedded ½″ deep into the tension face of each RC deck or column by grooving concrete, placing, and grouting the sensor with non-shrink cement. CS-100 Crackscope will be used to measure the crack width (local damage). In addition, BOTDR optical fiber sensors will be installed for performance comparison with the coaxial cable sensors since they constitute two types of continuous sensors currently available in the world.

The well-conceived test plan developed in Task 1 will be executed effectively to minimize the actual duration of field testing without sacrificing the quality of test data and setting back the project goals. To accommodate any unexpected situations, some flexibility needs to be built in the test plan. Past experiences indicate that communication is a key to make field tests efficient. In this case, the effective interaction between two groups (field instrumentation and validation

tests, and potential subcontracting for concrete cutting and heavy equipment lifting) is critical. Maintaining constant dialogues with the bridge decommissioning contractor is also important.

Task 4 Laboratory Calibration and Rebar Stress Prediction from Crack Data

For the purpose of laboratory calibrations, each coaxial cable sensor will be fabricated at least three feet longer than needed for field testing. The extra three feet will be cut and used for laboratory calibration. In this way, identical cable sensors will be used in laboratory and field testing. The cable sensors will be embedded at approximately ½″ deep into 3-ft long RC beams that will be tested under monotonic loads for the characterization of sensitivity, spatial resolution, and signal loss (Chen et al. 2004). The reflection coefficient measured from each sensor will be correlated with the crack width measured with a Peak CS-100 Crackscope (Brower et al. 2006). In addition, strain gauges will be attached to the tension reinforcing bars to measure the strain distribution along the bars close to the cable sensors. This set of results will allow the validation of a mechanical model to be used to predict the rebar stress condition based on the crack patterns on the surface of concrete member and the reinforcement design.

Task 5 Performance Comparison with Distributed Optical Fiber Measurements

The coaxial cable sensors are most suitable for crack detection while optical fiber sensors are used for strain and temperature measurement. Both will be instrumented both in laboratory tests of model structure members and field tests of the bridge deck and column. Their results will be correlated through a mechanical model that relates the crack to the strain field around. In addition, readings from strain gauges can further facilitate the understanding of strain field around cracks or validate the BOTDR measurements.

Schedule and Milestones

The Phase II project will be completed in 12 months. The project schedule and milestones are detailed in Table 2. Also included in Table 2 are four milestones, including test plan review, design review, data collection, and reporting.

Table 2 Project Schedule and Milestones

Task\Month	June	July	Aug	Sept	Oct	Nov	Dec	Jan	Feb	Mar	Apr	May
1		——▶①										
2		——▶②										
3				————▶③								
4						——————————————▶						
5	——————————————————————————————▶④											

Milestones: ① = test plan review, ② = design review, ③ = data collection, and ④ = reporting.

6 CONCLUDING REMARKS

The Phase II proposal will be prepared and submitted to NYSERDA and NYDOT for consideration. The execution of field tests of the select bridge will provide a unique set of test data for coaxial cable sensor and instrument validation as well as for their performance comparison with optical fiber sensors. The field proven technology has potential applications in several areas, including:

- Monitoring of surface and hidden cracks in structural members,
- Evaluation of deep foundations and shaft constructions, and
- Assessment of strengthened structural members of an existing bridge.

ACKNOWLEDGEMENT

REFERENCES

Bao, X., DeMerchant, M., Brown A., and Bremner, T. (2001), "Strain Measurement of the Steel Beam with the Distributed Brillouin Scattering Sensor", Health Monitoring and Management of Civil Infrastructure Systems, Steven B. Chase, A. Emin Aktan, Editors, Proceedings of SPIE, 4337, 223-233.

Brower, M., Z. Royer, G.D. Chen, D. Van Aken, and D. Pommerenke, "Distributed Cable Sensors for Structural Damage Detection: Implementation Issues," Proceedings of the 2006 ASCE Structures Congress, St. Louis, May 18-20, 2006.

Chen, G.D., H.M. Mu, D. Pommerenke, and J.L. Drewniak, "Damage Detection of Reinforced Concrete Beams with Novel Distributed Crack/Strain Sensors," *Structural Health Monitoring: an International Journal*, **3**(3), 2004, pp. 225-243.

Chen, G.D., B. Xu, R. McDaniel, X. Ying, D. Pommerenke, and Z. Wu, "Distributed Strain Measurement of a Large-scale Reinforced Concrete Beam-column Assembly under Cyclic Loading," Proceedings of the 12th SPIE Annual Symposium on Smart Structures and Materials, San Diego, California, March 6-10, 2005b, pp. 786-797.

Greene, G.G., A. Belarbi, and G.D. Chen, "Crack Mapping in RC Members Using Distributed Coaxial Cable Crack Sensors: Modeling and Application," *Smart Structures and Systems: an International Journal*, **1**(4), 2005.

Gu, X., Chen, Z. and Ansari, F. 2000. "Embedded Fiber Optic Crack Sensor for Reinforced Concrete Structures", ACI Structural Journal, 97(3), 468-476.

Horiguchi, T., Kurashima, T. and Tateda, M. (1989), "Tensile Strain Dependence of Brillouin Frequency Shift in Silica Optical Fibers", Photonics Technology letters, 1, 107-108.

Ishii,T., Wu, Z.S, and Horiuchi T. (2002), "Study on Characteristics of Strain Measurement with Optical Fiber", Transactions of the Japan Concrete Institute, 23,133-140.

Nikles, M., Briffod, F., Burke, R., and Lyons, G. (2005), "Greatly Extended Distance Pipeline Monitoring Using Fibre Optocs", Proceedings of 24th International Conference on Offshore Mechanics and Arctic Engineering,

Sun, S.S., D. Pommerenke, J.L. Drewniak, and G.D. Chen, "Signal Loss, Spatial Resolution, and Sensitivity of Long Coaxial Crack Sensors," Proceedings of the 11th SPIE Annual Symposium on Smart Structures and Materials, San Diego, California, March 11-18, 2004.

Wu, Z. S., Takahashi, T., Kino, H. and Hiramatsu, K. (2000), "Crack Measurement of Concrete Structures with Optic Fiber Sensing", Proc. Japan Concrete Institute, 22(1), 409-414.

Wu, Z.S., Takahashi, T. and Sudou, K. (2002), "An Experimental Investigation on Continuous Strain and Crack Monitoring with Fiber Optic Sensors", Concrete Research and Technology, 13(2), 139-148.

Wu, Z.S. and Xu B. (2002), "Infrastructural Health Monitoring with BOTDR Fiber Optic Sensing Technique", Proceedings of the 1st International Workshop on Structural Health Monitoring of Innovative Civil Engineering Structures, ISIS Canada Research Network, 217-226.